Downloaded from rsta.royalsocietypublishing.org

PHILOSOPHICAL TRANSACTIONS OF THE ROYAL SOCIETY A MATHEMATICAL, PHYSICAL & ENGINEERING SCIENCES

On the Oblique Reflexion and Transmission of Ocean Waves at Shore Fast Sea Ice

Colin Fox and Vernon A. Squire

Phil. Trans. R. Soc. Lond. A 1994 **347**, 185-218
doi: 10.1098/rsta.1994.0044

Email alerting service

Receive free email alerts when new articles cite this article - sign up in the box at the top right-hand corner of the article or click **here**

To subscribe to *Phil. Trans. R. Soc. Lond. A* go to:
http://rsta.royalsocietypublishing.org/subscriptions

This journal is © 1994 The Royal Society

Downloaded from rsta.royalsocietypublishing.org

On the oblique reflexion and transmission of ocean waves at shore fast sea ice†

By Colin Fox[1] and Vernon A. Squire[2]

[1]*Department of Mathematics, The University of Auckland, Private Bag 92019, Auckland, New Zealand*

[2]*Department of Mathematics and Statistics, University of Otago, P.O. Box 56, Dunedin, New Zealand*

Contents

A mathematical model is reported describing the oblique reflexion and penetration of ocean waves into shore fast sea ice. The arbitrary depth model allows all velocity potentials occurring in the open water region to be matched precisely to their counterparts in the ice-covered region. Matching is done using a preconditioned conjugate gradient technique which allows the complete solution to be found to a predefined precision. The model enables the reflexion and transmission coefficients at the ice edge to be found, and examples are reported for ice plates of different thicknesses. A critical angle is predicted beyond which no travelling wave penetrates the ice sheet; in this case the deflexion of the ice is due only to evanescent modes. Critical angle curves are provided for various ice thicknesses on deep, intermediate and shallow water. The strain field which is set up within

† This paper was produced from the authors' disk by using the TEX typesetting system.

Phil. Trans. R. Soc. Lond. A (1994) **347**, 185–218
Printed in Great Britain

© 1994 The Royal Society

The Royal Society is collaborating with JSTOR to digitize, preserve, and extend access to *Philosophical Transactions: Physical Sciences and Engineering.* www.jstor.org

Downloaded from rsta.royalsocietypublishing.org

the ice sheet due to the incoming waves is also discussed; principal strains are provided as are the strains normal to the ice edge. Finally the spreading function within the ice cover, and some consequences of this function to unimodal seas with realistic open water spreading functions, are reported with the aim of generalizing the work to model the effect of shore fast ice on an incoming directional wave spectrum of specified structure.

Nomenclature

a_n	coefficients of bounded evanescent modes in water
b_+	coefficients of first damped travelling mode
b_-	coefficients of second damped travelling mode
b_n	coefficients of bounded evanescent modes in the ice
f	frequency
f_m	frequency of peak in power spectral density
g	acceleration due to gravity
h	ice thickness
i	$\sqrt{-1}$
k	generic wave number in open water
k_y	wave number in y-direction, i.e. vertical
k_z	wave number in z-direction, i.e. parallel to ice edge
$\pm \mathrm{i}k_\mathrm{T}, \pm k_n$	roots of dispersion relation (2.17) for open water
k_T	travelling water wave number
k'_T	travelling water wave number in x-direction
k_n	evanescent water wave numbers
k'_n	evanescent water wave numbers in x-direction
$m = \rho_\mathrm{i} h$	mass per unit area of the ice plate
$r(x, z, \theta)$	radius of curvature of ice sheet at (x, z) in direction θ
$s(x, z, \theta)$	infinitesimal strain in direction θ at a point (x, z)
t	time
x	horizontal coordinate perpendicular to the ice edge
y	vertical (positive upwards from sea floor) coordinate
z	horizontal (along ice edge) coordinate
E	effective elastic modulus
E_o	incident energy density
E_i	transmitted energy density
$G_\mathrm{o}(\theta_\mathrm{o})$	open water spreading function
$G_\mathrm{i}(\theta_\mathrm{i})$	spreading function in ice sheet
H	water depth
$L = Eh^3/12(1-\nu^2)$	effective flexural rigidity
$P(x, z)$	atmospheric pressure on the water surface
$P_\mathrm{i}(x, z)$	differential pressure on the ice surface
I	coefficient of open water incident travelling wave
R	coefficient of open water reflected travelling wave
T	coefficient of travelling wave in ice-covered region
$\mathcal{E}$	the error integral defined by equation (2.21)

PHILOSOPHICAL TRANSACTIONS OF THE ROYAL SOCIETY A MATHEMATICAL, PHYSICAL & ENGINEERING SCIENCES
PHILOSOPHICAL TRANSACTIONS OF THE ROYAL SOCIETY A MATHEMATICAL, PHYSICAL & ENGINEERING SCIENCES

Downloaded from rsta.royalsocietypublishing.org

$\mathcal{R}$	amplitude reflexion coefficient
$\mathcal{T}$	amplitude transmission coefficient
ϵ	infinitesimal strain tensor at a point (x, z) in ice sheet
$\eta(x, z, t)$	displacement of the surface from equilibrium
κ	generic ice wave number
$\pm\mathrm{i}\kappa_{\mathrm{T}}, \pm\kappa_{\mathrm{D}}, \pm\kappa_{\mathrm{D}}^*, \pm\kappa_n$	roots of dispersion relation (2.19) for ice-covered region
κ_{T}	travelling ice wave number
κ'_{T}	travelling ice wave number in x-direction
$\kappa_{\mathrm{D}}, \kappa_{\mathrm{D}}^*$	damped ice travelling wave numbers
$\kappa'_{\mathrm{D}}, \kappa'^*_{\mathrm{D}}$	damped ice travelling wave numbers in x-direction
κ_n	evanescent ice wave numbers
κ'_n	evanescent ice wave numbers in x-direction
$\lambda = 2\pi/k$	wavelength
ν	Poisson's ratio
$\phi(x, y)$	(x, y) behaviour of complex velocity potential
$\phi_{\mathrm{o}}(x, y)$	open water complex velocity potential
$\phi_{\mathrm{i}}(x, y)$	ice-covered region complex velocity potential
$\omega = 2\pi/\mathrm{period}$	radian frequency
ρ	density of water
ρ_{i}	density of ice
θ	angle to normal at ice edge
θ_{o}	angle of incidence
θ_{i}	angle of transmission
$\overline{\theta_{\mathrm{o}}}$	mean (principal) angle of incidence
$\overline{\theta_{\mathrm{i}}}$	mean (principal) angle of transmission
ζ_{o}	complex surface displacement in open water
ζ_{i}	complex surface displacement in ice-covered region
$\Phi(x, y, z, t)$	complete velocity potential

1. Introduction

Along the coasts of the islands and landmasses of the Arctic and Antarctic Oceans, and especially within sheltered bays or inlets which may be protected from significant seas by pack ice or by their geography, sea water freezes during the winter months into a continuous, relatively featureless, floating sheet of sea ice known as fast ice. This fast ice often survives well into the spring until the pack ice departs, abandoning the ice sheet to local storms. Then, in most cases, the sheet will be broken up by incoming waves and swell to leave the sea surface free of ice for the cycle to begin again the following winter. In rare cases the fast ice can survive the summer intact, and can then continue its growth during subsequent winters until it becomes very thick (Wadhams 1986). In the Arctic Ocean it is then called sikussak by the Inuit. Ultimately this ice will also break up, though how this occurs is unknown.

Apart from the zone directly in contact with the landmass, the ice sheet varies little in thickness and usually has few cracks unless smaller islands are present within the fast ice sheet itself. At the coast there is a tide crack – as the ice-covered sea surface must still follow local tides – and there will often be rougher ice and pressure ridging or hummocking. It is also very common for cracks in the ice to

PHILOSOPHICAL TRANSACTIONS OF THE ROYAL SOCIETY A MATHEMATICAL, PHYSICAL & ENGINEERING SCIENCES
PHILOSOPHICAL TRANSACTIONS OF THE ROYAL SOCIETY A MATHEMATICAL, PHYSICAL & ENGINEERING SCIENCES

Downloaded from rsta.royalsocietypublishing.org

develop between islands, formed probably by local meteorological disturbances causing divergence and convergence of the ice sheet by coupling directly to the ice. Away from these features the sea ice has reasonably constant thickness and relatively homogeneous physical, and hence mechanical, properties in the horizontal plane. Through its thickness, however, properties vary markedly as the upper surface of the ice is at the ambient air temperature, whereas its underside is at the temperature of the seawater beneath. Thus there is a strong temperature gradient through the ice thickness. There is also a salinity gradient, caused by brine being trapped within the ice structure as it grows. Since this process of brine entrapment is rate dependent it will be influenced by the developing thickness of the ice sheet. The mechanical properties of sea ice have been found to depend on brine volume, which may be computed empirically from the temperature and salinity profiles through the sheet if these data are available (Frankenstein & Garner 1967). Fortunately for the modellers, Kerr & Palmer (1972) have shown that in so far as the elastic response of an ice sheet is concerned, a modified flexural rigidity may be defined which allows a fully homogeneous plate theory to be used.

The reflexion and transmission of incoming ocean waves at an ice edge and the character of the so-called 'ice-coupled' wave modes within the ice sheet are the motivation for this paper. One of the authors (V.A.S.) has observed ice-coupled waves on many occasions, and it is striking that there is significant regularity and repeatability in their properties from location to location, and from year to year. Typically, incoming waves are partly reflected at the seaward margin of the ice sheet, allowing some wave energy to be refracted into the ice as a propagating wave travelling beneath the plate. Other modes are also generated and these will be discussed later. The reflected waves lead to particularly hazardous seas off the edge (Squire & Fox 1990), and this is especially true when the waves are incident at a fairly large angle as a critical angle exists beyond which total external reflexion of the sea waves must take place (Squire 1984 *b–d*). Within the ice plate the transmitted wave, and additional modes which rapidly decay with penetration, cause the sheet to flex significantly at an amplitude which depends on factors such as the incident wave amplitude, the mechanical properties of the ice, and the ice thickness. This flexing, which can often be observed with the eye, leads to strains and therefore stresses in the ice sheet which may be large enough to cause fracture. When fracture does occur, cracks form at well-defined, equally spaced intervals back from the ice edge. Based on the few observations that are available, crack spacing is strongly correlated with ice thickness.

Wave propagation in ice-infested seas, whether through pack ice or beneath shore fast sea ice, is not a new problem. Indeed, it is known even to have been studied theoretically as early as 1887 (Greenhill 1887), and there are accounts of observations by whaling ships which predate this by decades. However, it is only recently that a precise solution has been reported (Fox & Squire 1990, 1991*a*), all previous models being based on an incomplete and hence approximate solution space. The level of approximation involved is discussed in (Fox & Squire 1990) in relation to the calculation of the reflexion and transmission coefficients at normal incidence, where it is shown that the approximate theories do not perform well at moderate ice thicknesses for wave periods less than about 12 s and are hopeless at short periods. Moreover the approximation becomes worse as ice thickness increases, or water depth decreases. The current paper considerably extends the work of Fox & Squire (1990, 1991*a*) and some additional studies reported in

PHILOSOPHICAL TRANSACTIONS OF THE ROYAL SOCIETY A MATHEMATICAL, PHYSICAL & ENGINEERING SCIENCES

PHILOSOPHICAL TRANSACTIONS OF THE ROYAL SOCIETY A MATHEMATICAL, PHYSICAL & ENGINEERING SCIENCES

Downloaded from rsta.royalsocietypublishing.org

Fox & Squire (1991*b*) and Squire & Fox (1991), developing the case of oblique incidence and some of its implications. The present work also draws on some of the early publications on wave–ice interaction, and it is for this reason that a short historical résumé is included.

(*a*) *Historical résumé*

In modelling an ice sheet as a thin elastic beam on a fluid foundation, Greenhill (1887) set the scene for many subsequent publications about wave propagation beneath ice; he was the first to show, for example, that ice-coupled waves disperse in a different manner from surface gravity waves in open water. Ewing *et al.* (1934), Ewing & Crary (1934), and later Press *et al.* (1951), Press & Ewing (1951) and Oliver *et al.* (1954), developed Greenhill's ideas further in a series of field experiments and analyses to study elastic and flexural ice-coupled wave propagation in ice of various types, including the compressibility of the water column and treating the ice as a plate rather than as a beam. The waves were generated artificially by detonation blasts, and were used to measure the high frequency Young's modulus of ice. Roethlisberger (1972) summarizes this programme of seismic work.

A renewed interest in ice-coupled waves of natural origin developed in the 1950s with a sequence of papers concerned with the boundary value problem at the ice edge, and the calculation of the reflexion and transmission coefficients (Peters 1950; Weitz & Keller 1950; Keller & Goldstein 1953; Shapiro & Simpson 1953; Keller & Weitz 1953). These authors treat the ice as a floating material of uniform surface density with no elastic properties or viscosity, the so-called mass-loading model; they are very useful papers for comparison with the more complete theory presented here as they solve the reduced problem completely and explain certain limiting features. Furthermore, the simpler theory may offer a reasonable model for wave propagation through frazil or pancake ice; Wadhams & Holt (1991) have recently interpreted some synthetic aperture radar observations using this approach.

Although the elastic thin plate surface boundary condition for the ice sheet as first proposed by Greenhill was reintroduced by Hendrickson & Webb (1963) and subsequently by Wadhams (1973, 1986) and Squire (1978, 1984*a*,*b*), the (normal incidence) reflexion and transmission coefficients derived were only found approximately, as the incomplete set of velocity potentials employed could only be matched at the surface. The inherent flaw in the model was recognized by each of the authors, but only Wadhams (1973, 1986) attempted to partly correct for the mismatch by including an additional potential. Ice-coupled waves have also been studied by Bates & Shapiro (1980), Grande (1983), Green (1985), by several Russian authors (e.g. Timokov and Kheisin 1987), and for large amplitude waves, by Forbes (1986, 1988). Recently, some authors (e.g. Weber 1987, Liu and Mollo-Christensen 1988, Lui *et al.* 1991*a*,*b*, 1992, Squire & Fox 1991) have used the ice-coupled wave analogy to represent wave propagation through pack ice, i.e. they have modelled a collection of interacting discrete sea ice floes as a continuum.

It is the report of Evans & Davies (1968), though a rather obscure publication, that offers the principal ingress into solving the boundary value problem representing waves entering a region covered with shore fast ice. These authors, in fact, attacked the complete problem and used the Weiner–Hopf technique to obtain

Downloaded from rsta.royalsocietypublishing.org

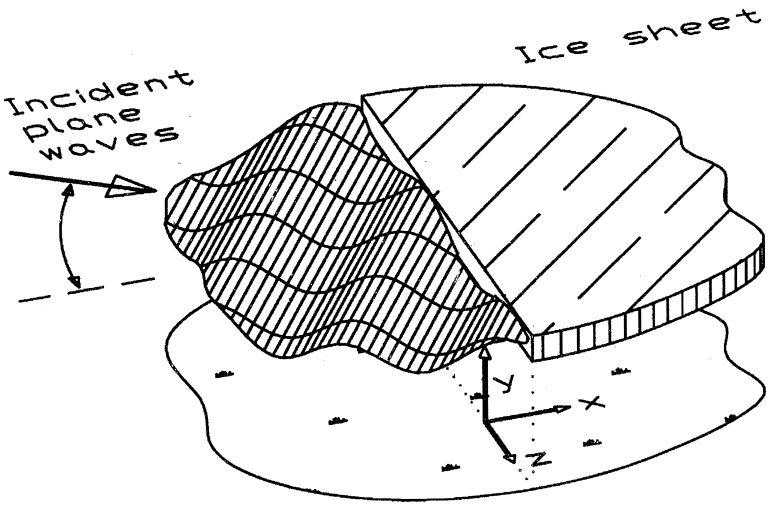

Figure 1. Schematic showing plane ocean waves obliquely incident on a sheet of shore fast sea ice. The coordinate system used in the model is located on the sea floor beneath the ice edge as shown.

its formal solution. Their solution is, however, computationally formidable and results could only be found for very simple geometries. The present paper draws on parts of Weitz & Keller (1950), Keller & Weitz (1953), and Evans & Davies (1968), extending and developing their ideas but using an entirely novel method of solution which allows us to obtain the complete solution to the appropriate boundary value problem.

2. The mathematical model

In this section the mathematical model is derived to describe small amplitude ocean waves propagating from the open ocean into a floating ice sheet. In the small amplitude limit the differential equations become linear, allowing superposition techniques to be used. Initially the simple case of single frequency, and hence steady state, excitation will be considered and the differential equation is derived with that assumption. The solution for more complicated types of excitation, such as an incoming directional wave spectrum, can be found by superposing solutions of the simpler system.

(a) *Geometry*

A semi-infinite ice sheet of thickness h floats at the surface of water of constant depth H. A region including part of the ice edge is depicted in figure 1. The figure also shows the coordinate axes x, y, z and an obliquely incident plane ocean wave. The sea bottom is the plane $y = 0$, the equilibrium sea surface is the plane $y = H$, and so the water occupies the three-dimensional region defined by $-\infty < x < \infty$, $0 < y \leqslant H$, $-\infty < z < \infty$. The ice sheet floats on the water surface in the semi-infinite region $0 \leqslant x < \infty$, $y = H$, $-\infty < z < \infty$.

Downloaded from rsta.royalsocietypublishing.org

(*b*) *The boundary value problem*

As viscous effects in oceanic flow of this amplitude on this scale are negligible (Phillips 1977), it follows from Kelvin's theorem that the flow is irrotational and hence it may be written as the gradient (in the space variables) of some scalar field $\Phi(x, y, z, t)$ called the velocity potential. The incompressibility of water, and the lack of sources within the region then implies that Φ satisfies Laplace's equation, i.e.

$$\nabla^2 \Phi = 0, \tag{2.1}$$

at all points and for all time.

(i) *Bottom boundary condition*

The component of velocity normal to any solid boundaries must vanish. Hence, at the sea floor the velocity potential satisfies the condition

$$\left.\frac{\partial \Phi}{\partial y}\right|_{y=0} = 0. \tag{2.2}$$

(ii) *Free-surface boundary condition*

Under the small amplitude assumption, the kinematic condition at the surface of the ocean becomes the linear condition at the equilibrium surface (Stoker 1957),

$$\frac{\partial \eta}{\partial t} = \frac{\partial \Phi}{\partial y}, \quad \text{for } y = H, \tag{2.3}$$

where $\eta(x, z, t)$ is the displacement of the surface from equilibrium at position x, z at time t.

The dynamic condition at the ocean surface can similarly be linearized and stated in terms of the potential at the equilibrium surface giving (Stoker 1957)

$$\frac{\partial \Phi}{\partial t} + \frac{P}{\rho} + g\eta = 0, \quad \text{for } y = H, \tag{2.4}$$

where $P(x, z)$ is the pressure at the surface of the water.

The pressure at the free surface in the region $-\infty < x < 0$ is equal to the constant atmospheric pressure and so η may be eliminated from equations (2.3) and (2.4) to give

$$\frac{\partial^2 \Phi}{\partial t^2} = -g\frac{\partial \Phi}{\partial y}, \quad \text{for } -\infty < x < 0, \quad y = H. \tag{2.5}$$

This is the boundary condition that the small amplitude potential must satisfy at the free surface of the ocean.

(iii) *Ice-covered surface boundary condition*

Assuming no cavitation between the ice sheet and the ocean surface, the linearized kinematic and dynamic conditions of equations (2.3) and (2.4) also hold at the equilibrium surface of the ice-covered region $0 < x < \infty$, $y = H$. In this case η is the transverse (i.e. y-direction) displacement of the ice sheet, and $P(x, z)$ is the pressure at the surface due to the atmosphere, the static pressure of the ice sheet and the dynamic pressure due to the inertia and stiffness, etc., of the ice sheet. It is assumed that the ice sheet acts as a thin, linearly elastic plate of

PHILOSOPHICAL TRANSACTIONS OF THE ROYAL SOCIETY A MATHEMATICAL, PHYSICAL & ENGINEERING SCIENCES
PHILOSOPHICAL TRANSACTIONS OF THE ROYAL SOCIETY A MATHEMATICAL, PHYSICAL & ENGINEERING SCIENCES

Downloaded from rsta.royalsocietypublishing.org

uniform mass density ρ_i and thickness h. The choice of a linear elastic model is consistent with earlier formulations. Linearity is justified because of the small curvatures involved as the ice sheet bends to the passing waves; elasticity is justified because of the oscillatory nature of the problem which does not allow anelastic processes to act in any significant way. The extension to a linear viscoelastic plate theory is not difficult (Squire & Fox 1992). The validity of a thin plate theory has been demonstrated by Fox & Squire (1991*b*). With these assumptions the displacement η from equilibrium is related to the differential pressure P_i by the equation (Timoshenko & Woinowsky-Krieger 1970)

$$P_i = L\nabla_{xz}^4\eta + m\left(\frac{\partial^2\eta}{\partial t^2} + g\right), \tag{2.6}$$

where $L = Eh^3/12(1-\nu^2)$ is the flexural rigidity of the ice, E is the effective (i.e. low strain rate) average Young's modulus for the ice, ν is Poisson's ratio, $m = \rho_i h$ is the mass per unit surface area of the ice sheet, and $\nabla_{xz}^2 = \partial^2/\partial x^2 + \partial^2/\partial z^2$ is the Laplacian in the plane of the ice sheet.

When the surface pressure $P(x,z)$ in the linearized dynamic condition (2.4) is equated to the sum of P_i and the constant atmospheric pressure, we find that the velocity potential must satisfy the relationship,

$$\left(L\nabla_{xz}^4 + m\frac{\partial^2}{\partial t^2} + \rho g\right)\frac{\partial\Phi}{\partial y} + \rho\frac{\partial^2\Phi}{\partial t^2} = 0, \quad \text{for } y = H, \quad 0 \leqslant x < \infty, \tag{2.7}$$

where again equation (2.3) has been used to eliminate η.

(iv) *Ice edge boundary condition*

Equation (2.7) is not, in itself, sufficient to determine the motion of the ice plate uniquely. Additional conditions concerning the bending moment and the shearing force at the edge of the ice sheet must be imposed. The precise quantities that must be prescribed at the boundary to completely define the motion can be found by considering the boundary conditions which arise as the difference between the differential equation and the variational problem that it leads to.

In Appendix A we develop the natural boundary conditions (A 2) and (A 3) for the ice sheet corresponding to the requirement that no work is done by, or to, the edge of the sheet. In terms of the potential, using equation (2.3), these boundary conditions are:

$$L\frac{\partial^2}{\partial x\partial y}\nabla_{xz}^2\Phi + (1-\nu)L\Phi_{xyzz} = 0, \quad \text{for } x = 0^+, \quad y = H, \quad -\infty < z < \infty, \tag{2.8}$$

and

$$L\left(\Phi_{xxy} + \nu\Phi_{yzz}\right) = 0, \quad \text{for } x = 0^+, \quad y = H, \quad -\infty < z < \infty. \tag{2.9}$$

(v) *The system for wavelike forcing*

We suppose now that the forcing of the system has sinusoidal dependence in z and t, and use complex notation to represent phasors for the time dependence ($e^{i\omega t}$) and the z-dependence ($e^{ik_z z}$). As the system is linear and is shift invariant in both time and the z variables, it follows that the resulting velocity potential can be separated as follows:

$$\Phi(x,y,z,t) = \phi(x,y)e^{i\omega t}e^{ik_z z}, \tag{2.10}$$

Downloaded from rsta.royalsocietypublishing.org

for some, possibly complex, function $\phi(x, y)$. Note that this development does not preclude forcing by an incoming sea composed of waves of many frequencies as superposition may be used. Indeed since any finite-energy forcing function can be decomposed into a linear combination of sinusoidal forcings, equation (2.10) does not restrict in any way the class of forcing functions that we may wish to consider.

Substituting equation (2.10) into equations (2.1), (2.2) and (2.5), we find that $\phi(x, y)$ must satisfy the Helmholtz equation within the water,

$$\left(\frac{\partial^2}{\partial x^2} + \frac{\partial^2}{\partial y^2} - k_z^2\right)\phi = 0, \quad \text{for } -\infty < x < \infty, \quad 0 < y \leqslant H, \tag{2.11}$$

together with the sea floor boundary condition,

$$\left.\frac{\partial \phi}{\partial y}\right|_{y=0} = 0, \tag{2.12}$$

and a free surface boundary condition,

$$g\frac{\partial \phi}{\partial y} - \omega^2 \phi = 0, \quad \text{for } -\infty < x < 0, \quad y = H. \tag{2.13}$$

The condition at the ice-covered ocean surface becomes, from equation (2.7),

$$\left(L\left(\frac{\partial^2}{\partial x^2} - k_z^2\right)^2 - m\omega^2 + \rho g\right)\frac{\partial \phi}{\partial y} - \rho\omega^2\phi = 0, \quad \text{for } y = H, \quad 0 < x < \infty. \tag{2.14}$$

Finally, the boundary conditions at the ice edge arising from incoming ocean waves are, from equation (2.8) and (2.9),

$$\left(\frac{\partial^3}{\partial x^3} - (2-\nu)\,k_z^2\frac{\partial}{\partial x}\right)\frac{\partial \phi}{\partial y} = 0, \quad \text{for } x = 0^+, \quad y = H, \tag{2.15}$$

and

$$\left(\frac{\partial^2}{\partial x^2} - \nu k_z^2\right)\frac{\partial \phi}{\partial y} = 0, \quad \text{for } x = 0^+, \quad y = H. \tag{2.16}$$

Equations (2.11) to (2.16) pose a well-defined, classical boundary value problem for the potential $\phi(x, y)$ which we solve numerically to an arbitrary prescribed precision.

(*c*) *Method of solution*

(i) *Representing the potential as modes*

By separating variables on either side of the line $x = 0$, $0 < y < H$, a complete set of potentials can be found; each satisfying the differential equation (2.11), the bottom boundary condition (2.12), and either the free surface condition (2.13) or the ice-covered surface condition (2.14). These potentials are the modes of the system and any solution of the model can be represented as a combination of these modes. Each mode can be written in the form $\phi(x, y) = \mathrm{e}^{k_x x}\mathrm{e}^{\pm \mathrm{i} k_y y}$, where $k_x^2 - k_y^2 - k_z^2 = 0$ must hold in order to satisfy differential equation (2.11). Pairs of these modes may be combined to give the equivalent set of modes $\phi(x, y) = \mathrm{e}^{k_x x}\sin(k_y y)$ and $\phi(x, y) = \mathrm{e}^{k_x x}\cos(k_y y)$. However, boundary condition (2.12) at

PHILOSOPHICAL TRANSACTIONS OF THE ROYAL SOCIETY A MATHEMATICAL, PHYSICAL & ENGINEERING SCIENCES

Downloaded from rsta.royalsocietypublishing.org

the sea floor rules out the modes with $\sin(k_y y)$ y-dependence, leaving only those with $\cos(k_y y)$ y-dependence. Only certain values of k_x and k_y give rise to modes which also satisfy either of the boundary conditions at the sea surface.

For convenience, we note that our choice of mode implies an equivalence of operators as follows:

$$\nabla^2_{xz} \equiv k_x^2 - k_z^2 \qquad \text{and} \qquad \nabla^4_{xz} \equiv \left(k_x^2 - k_z^2\right)^2.$$

Hence, letting $k = k_y$, we obtain $k^2 = k_x^2 - k_z^2$, and so $\nabla^2_{xz} \equiv k^2$ and $\nabla^4_{xz} \equiv k^4$. Thus, given k_z and k we have

$$k_x = \pm\sqrt{k^2 + k_z^2}.$$

We are concerned with cases where k_z is real so that k_z^2 is real and positive. The wavenumber k, however, may take on a range of values and k_x can be real, pure imaginary, or sometimes complex. When k_x is real, the mode which has oscillatory behaviour in the z-direction decays (or grows) exponentially in a direction normal to the ice edge, i.e. in the x-direction. Such a mode is said to be evanescent, and transports no energy into the ice sheet. When k_x is pure imaginary the mode has sinusoidal dependence normal to the ice edge, and in this case it represents a travelling plane wave with (real and positive) wavenumber k, wavelength $\lambda = 2\pi/k$, which propagates at an angle $\theta_o = \arctan(k_z/\mathrm{Im}k_x)$ to the x-axis.

(ii) *Open sea region*

For $-\infty < x < 0$ the modes must satisfy the open sea condition (2.13) which occurs if k satisfies the dispersion equation

$$k\tan(kH) = -\omega^2/g. \tag{2.17}$$

This equation has two pure imaginary roots $\pm ik_T$ (where $k_T > 0$) corresponding to travelling plane waves propagating with positive and negative x components, and infinitely many real roots $\pm k_n$ $(n = 1, 2, \ldots)$, where $(n - \frac{1}{2})\pi/H < k_n < n\pi/H$, corresponding to evanescent modes. Since the y-dependence of these modes satisfies a self-adjoint boundary value problem it follows that the modes form a complete set and are orthogonal for differing values of k^2.

We consider only those roots of the dispersion equation which give rise to bounded modes for the open sea region $-\infty < x < 0$. Roots $\pm ik_T$ give the modes

$$e^{\pm ik'_T x}\cosh(k_T y), \qquad \text{where} \qquad k'_T = \sqrt{k_T^2 - k_z^2},$$

and for ocean wave forcing we require $k_z < k_T$ (note $k_z = k_T \sin\theta_o$). Then k'_T is real and positive, and the mode represents a travelling plane wave. For each n the real root k_n gives the mode

$$e^{k'_n x}\cos(k_n y), \qquad \text{where} \qquad k'_n = \sqrt{k_n^2 + k_z^2},$$

which is always evanescent.

Thus any bounded potential in the open sea region $-\infty < x < 0$ may be written as

$$\phi_o = \left(Ie^{-ik'_T x} + Re^{ik'_T x}\right)\cosh k_T y + \sum_{n=1}^{\infty} a_n e^{k'_n x}\cos k_n y, \tag{2.18}$$

Downloaded from rsta.royalsocietypublishing.org

where I and R are the complex coefficients of the travelling waves propagating with positive and negative x components respectively, and $\{a_n\}$ is the set of coefficients of the bounded evanescent modes.

(iii) *Ice-covered region*

In the ice-covered region, $0 \leqslant x < \infty$ we write the modes as $\phi(x, y) = \mathrm{e}^{\kappa_x x}\cos(\kappa y)$, replacing k by κ to distinguish between the two regions. The wave number κ must satisfy the more complicated dispersion equation:

$$\kappa \tan \kappa H = -\frac{\rho\omega^2}{L\kappa^4 - m\omega^2 + \rho g}. \tag{2.19}$$

This dispersion equation also has two imaginary roots $\pm \mathrm{i}\kappa_\mathrm{T}$ ($\kappa_\mathrm{T} > 0$) corresponding in general to travelling waves, four complex roots occurring as plus and minus a complex conjugate pair $\pm\kappa_\mathrm{D}$ and $\pm\kappa_\mathrm{D}^*$ (κ_D has positive real and imaginary parts) corresponding to damped travelling waves, and infinitely many real roots $\pm\kappa_n$ ($n = 1, 2, \ldots$), where in general $(n-\frac{1}{2})\pi/H < \kappa_n < (n+\frac{1}{2})\pi/H$, each giving an evanescent mode. The y-variable boundary value problem for these modes is not self-adjoint and in general these modes are not orthogonal. However, they do form a complete set for functions satisfying the same boundary value problem.

Again we consider only the roots of dispersion equation (2.19) giving rise to bounded modes. So the allowable modes for the ice-covered region, $0 \leqslant x < \infty$ are as follows:

The two imaginary roots $\pm \mathrm{i}\kappa_\mathrm{T}$ give the modes

$$\mathrm{e}^{\pm \mathrm{i}\kappa'_\mathrm{T} x}\cosh(\kappa_\mathrm{T} y), \qquad \text{where} \qquad \kappa'_\mathrm{T} = \sqrt{\kappa_\mathrm{T}^2 - k_z^2}.$$

When κ'_T is real these modes represent travelling waves. However, when $k_z > \kappa_\mathrm{T}$, κ'_T is pure imaginary and the modes are evanescent. Only the evanescent mode which decays with penetration into the ice cover is an allowable bounded mode. The onset of a pure imaginary κ'_T for ocean wave forcing corresponds to a critical incidence angle, and total reflexion of the incoming wave.

The two complex roots κ_D and κ_D^* lead to the two modes

$$\mathrm{e}^{\kappa'_\mathrm{D} x}\cos(\kappa_\mathrm{D} y) \text{ and } \mathrm{e}^{\kappa'^*_\mathrm{D} x}\cos(\kappa^*_\mathrm{D} y), \qquad \text{where} \qquad \kappa'_\mathrm{D} = \sqrt{\kappa_\mathrm{D}^2 - k_z^2},$$

and the branch of the square root is chosen to ensure that $\kappa'^*_\mathrm{D} = \kappa_\mathrm{D}$ when $k_z = 0$. Note also that $\mathrm{Re}(\kappa'_\mathrm{D}) > \mathrm{Im}(\kappa'_\mathrm{D})$ always.

For each n the real root κ_n gives the mode

$$\mathrm{e}^{\kappa'_n x}\cos(\kappa_n y), \qquad \text{where} \qquad \kappa'_n = \sqrt{\kappa_n^2 + k_z^2},$$

which is always evanescent.

Hence any relevant potential in the ice-covered region, $x > 0$, can be written

$$\phi_\mathrm{i} = T\mathrm{e}^{-\mathrm{i}\kappa'_\mathrm{T} x}\cosh\kappa_\mathrm{T} y + b_+\mathrm{e}^{-\kappa'_\mathrm{D} x}\cos\kappa_\mathrm{D} y + b_-\mathrm{e}^{-\kappa'^*_\mathrm{D} x}\cos\kappa^*_\mathrm{D} y + \sum_{n=1}^{\infty} b_n \mathrm{e}^{-\kappa'_n x}\cos\kappa_n y, \tag{2.20}$$

where T, b_+, b_- and $\{b_n\}$ are the complex coefficients of the various modes. The

Downloaded from rsta.royalsocietypublishing.org

potential in this region must also, of course, satisfy the relevant ice edge boundary conditions.

(iv) *Matching across the plane* $x = 0$, $0 < y < H$, $-\infty < z < \infty$

A solution of the boundary value problem can be found by matching the potentials ϕ_o and ϕ_i on the plane $x = 0$, $0 < y < H$, $-\infty < z < \infty$, while ensuring that the remaining boundary conditions are satisfied. The natural quantities to equate across the matching boundary are the potential ϕ and its normal derivative $\partial\phi/\partial x$. Matching is achieved by minimizing the error integral,

$$\mathcal{E} = \int_0^H |\phi_i - \phi_o|^2 \, dy + \mu \int_0^H \left| \frac{\partial \phi_i}{\partial x} - \frac{\partial \phi_o}{\partial x} \right|^2 dy, \tag{2.21}$$

evaluated at $x = 0$. In this expression the constant μ is a weighting term included to improve convergence, and which empirically is set to 10 in most cases. The solution to the wave forcing problem is then found by minimizing $\mathcal{E}$ subject to three extra conditions: the ice edge boundary conditions (2.15) and (2.16); and an additional condition which – without loss of generality – restricts the incoming wave in ϕ_o to have unit amplitude displacement. The two edge conditions give rise to two linear equations relating the coefficients of ϕ_i in equation (2.20).

To facilitate the required calculations, the infinite sums in equations (2.18) and (2.20) are terminated at some finite N, say, i.e. the first N evanescent modes only are included. The matching is performed for a sequence of increasing N until the solution has converged to its final value. Using the property that the error, $\mathcal{E}$, is a quadratic form in the real and imaginary parts of the coefficients I, R, $\{a_n\}$, T, b_+, b_- and $\{b_n\}$, the minimization is performed, with respect to these coefficients, using a preconditioned linear conjugate gradient algorithm (Gill *et al.* 1981) restricted to the affine subspace in which the three extra conditions are satisfied.

An independent check is made on the resulting potentials to ensure that they represent a system in energy balance. A relationship between the respective amplitudes of the travelling waves can be established by equating an energy flux in the outward travelling plane waves to the forcing energy flux (Evans & Davies 1968). Denoting the amplitude reflexion and transmission coefficients by $\mathcal{R}$ and $\mathcal{T}$ respectively, and using

$$\mathcal{R} = \frac{|R|}{|I|} \quad \text{and} \quad \mathcal{T} = \left(\frac{\kappa_T \sinh \kappa_T H}{k_T \sinh k_T H} \right) \frac{|T|}{|I|},$$

the relationship is

$$D\,\mathcal{T}^2 + \mathcal{R}^2 = 1, \tag{2.22}$$

where

$$D = \frac{\mathrm{Re}(\kappa_T') k_T^2 \sinh 2k_T H}{\mathrm{Re}(k_T') \kappa_T^2 \sinh 2\kappa_T H} \times \left\{ \frac{2\kappa_T H (L\kappa_T^4 + \rho g - m\omega^2) + \sinh 2\kappa_T H (5L\kappa_T^4 + \rho g - m\omega^2)}{\rho g (2k_T H + \sinh 2k_T H)} \right\}. \tag{2.23}$$

Note that this expression differs slightly from the expression given by Evans & Davies (1968) which is in error for obliquely incident waves.

PHILOSOPHICAL TRANSACTIONS OF THE ROYAL SOCIETY A MATHEMATICAL, PHYSICAL & ENGINEERING SCIENCES
PHILOSOPHICAL TRANSACTIONS OF THE ROYAL SOCIETY A MATHEMATICAL, PHYSICAL & ENGINEERING SCIENCES

Downloaded from rsta.royalsocietypublishing.org

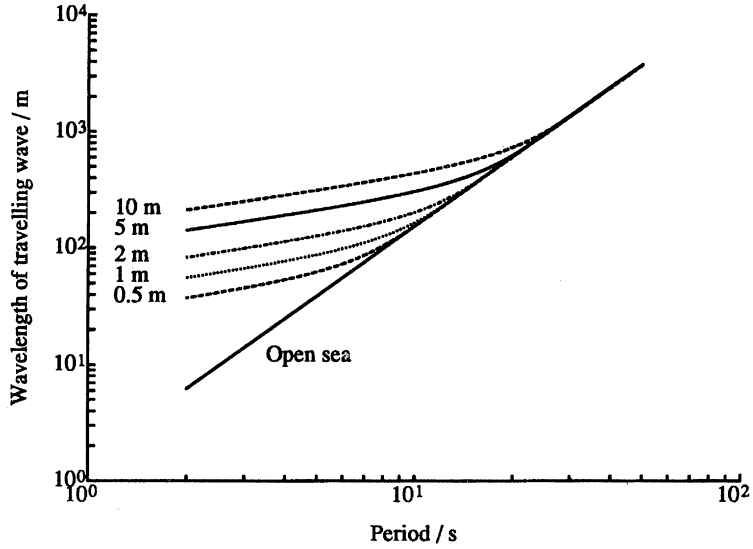

Figure 2. Wavelength of deep water travelling wave for a range of periods at various thicknesses.

3. Features of the model

(*a*) *Constants used in the model*

In subsequent calculations the following constants are used: $E = 6$ GPa, $\nu = 0.3$, $g = 9.8$ m s^{-2}, $\rho = 1025.0$ kg m^{-3}, and $\rho_i = 922.5$ kg m^{-3}.

(*b*) *Deep water*

The case of deep water can be treated by considering the depth H to be arbitrarily large. Since the roots of the dispersion equations corresponding to travelling waves $\pm ik_T$ and $\pm i\kappa_T$ are imaginary, the terms $\tan(ik_T H)$ and $\tan(i\kappa_T H)$ in equations (2.17) and (2.19), respectively, can be taken to equal i. Thus the deep water travelling wave number for ocean waves is

$$k_T = \omega^2/g, \tag{3.1}$$

while the deep water travelling wave number for ice-coupled waves is the positive real root of

$$L\kappa_T^5 + (\rho g - m\omega^2)\kappa_T - \rho\omega^2 = 0. \tag{3.2}$$

It should be noted that the approximation $\tan(kH) = i$ does not hold for the real roots corresponding to evanescent modes, and consequently the two deep water dispersion relations do not correctly predict the continuum of evanescent modes which exist in the infinite depth limit.

The wavelength of the open sea and ice-coupled travelling waves, for a range of periods and various ice thicknesses, is shown in figure 2. The wavelength of the ice-coupled wave is almost always greater than the wavelength of the ocean wave of the same period, and the wavelength increases with increasing ice thickness. For a given ice thickness the wavelength of the ice-coupled travelling wave approaches that of the travelling wave in the open ocean as period increases. At sufficiently long period the wavelength curves for the open sea and ice-coupled travelling

Downloaded from rsta.royalsocietypublishing.org

waves intersect, and the wavelength in the water exceeds that in the ice by a small amount. The approach and subsequent intersection of the curves is a function of ice thickness. The intersection appears to be due to the fact that at long wave periods the stiffness of the ice sheet is negligible and the ice-coupled wave effectively degenerates to a simple surface gravity wave modified slightly by the effect of the mass-loading term, i.e. the model reverts to a mass-loading model as the wave numbers become very small. In this limit $\kappa_T \to k_T/(1 - mk_T/\rho)$, so that the wavelength in ice becomes less than the wavelength in water. The mass-loading parametrization of an ice cover is the subject of several papers published some 40 years ago (Peters 1950; Weitz & Keller 1950; Shapiro & Simpson 1953; Keller & Weitz 1953), and more recently it has been used in connexion with the modelling of frazil and pancake ice by Wadhams & Holt (1991).

(c) *The critical angle*

The z-components of the open water wave number k_T and its counterpart in the ice κ_T are equal. This provides a wave–ice-interaction equivalent to Snell's law as follows:

$$k_T \sin\theta_o = \kappa_T \sin\theta_i, \tag{3.3}$$

where the dispersion relations (2.17) and (2.19) provide values for the wave numbers k_T and κ_T. It is of interest to consider the relative magnitude of these wave numbers. If $k_T < \kappa_T$ then $\sin\theta_i < \sin\theta_o$, and the transmitted travelling wave is refracted towards the normal at the ice edge. If, on the other hand, $k_T > \kappa_T$ then $\sin\theta_i > \sin\theta_o$ and the travelling wave is refracted away from the normal. In the present context the former case only occurs when the wave numbers are very small and the most common situation is $k_T > \kappa_T$, as seen in figure 2. In that case the angle of transmission θ_i is always greater than or equal to the angle of incidence θ_o. But $\theta_i \leqslant 90°$ so that a natural limit to the angle of incidence exists, beyond which propagation into the ice cover cannot take place. This occurs when $\theta_o = \arcsin(\kappa_T/k_T)$, thereby defining a critical angle for waves entering an ice sheet.

Critical angle curves for several ice thicknesses are shown in figures 3–5 for deep (1000 m), intermediate (100 m) and shallow (10 m) water respectively. Taking a typical curve, for example the curve for 1 m of ice on deep water (figure 3), the plots are interpreted as follows. To the right of each curve, the incoming wave generates a transmitted ice-coupled travelling wave mode which propagates into the ice cover. Along and to the left of each curve the incoming waves are perfectly reflected from the ice margin, and no propagating ice-coupled mode is generated within the ice sheet. The thicker the ice sheet, the more likely it is that the critical angle will be exceeded since the individual critical curves move towards longer periods as ice thickness is increased. The fine structure of each curve is also altered qualitatively by ice thickness and by water depth. Shallow water tends to produce curves which are concave down, whereas deep water produces curves which are concave up. In figure 4 especially, the plotted 2–30 s period range includes deep water at short periods and shallow water at long periods, and an inflexion point is evident in all curves. Curves meet the 90° angle of incidence line vertically in all cases since $\kappa_T \to k_T$ as the incoming wave approaches grazing incidence.

PHILOSOPHICAL TRANSACTIONS OF THE ROYAL SOCIETY A MATHEMATICAL, PHYSICAL & ENGINEERING SCIENCES

PHILOSOPHICAL TRANSACTIONS OF THE ROYAL SOCIETY A MATHEMATICAL, PHYSICAL & ENGINEERING SCIENCES

Downloaded from rsta.royalsocietypublishing.org

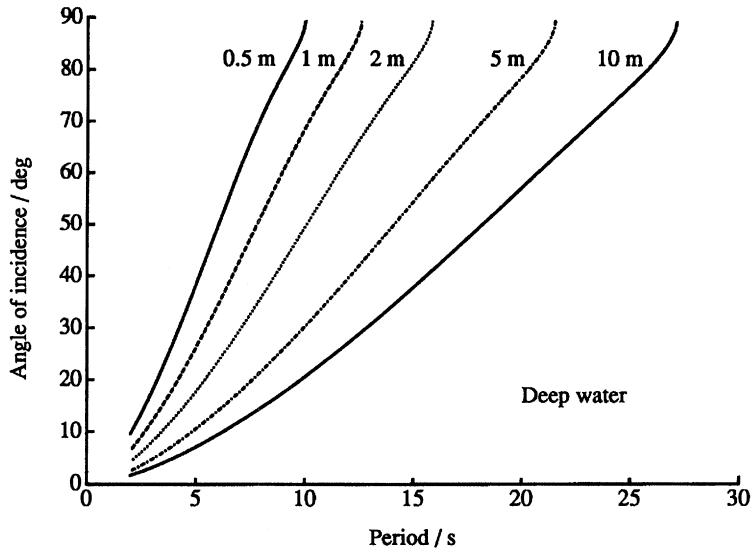

Figure 3. Critical angle curves at various thicknesses for deep water.

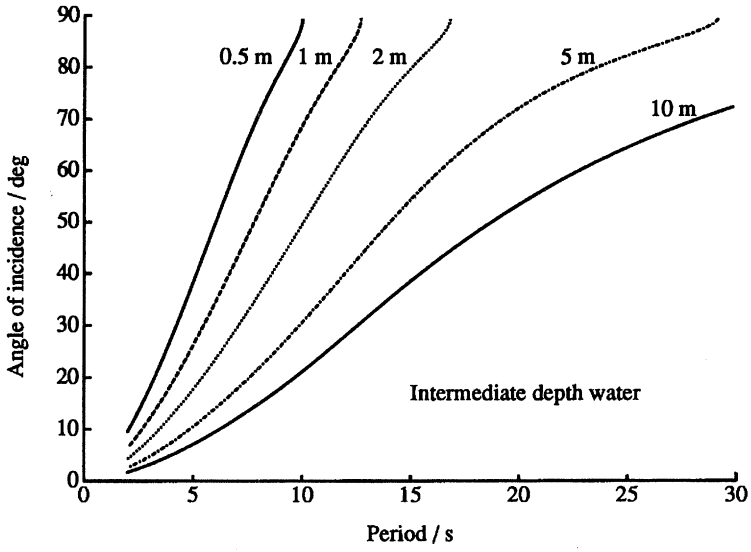

Figure 4. Equivalent curves to figure 3 for water of intermediate depth (100 m).

(*d*) *Surface displacements*

For a given potential ϕ the associated surface displacement η is given by substituting equation (2.10) into equation (2.3). For sinusoidal forcing (cf. equation (2.10)) $\eta(x, z, t)$ can be represented as (the real part of) the complex function $\zeta(x)\mathrm{e}^{\mathrm{i}\omega t}\mathrm{e}^{\mathrm{i}k_z z}$ where the x-dependence is given by

$$\zeta(x) = \frac{1}{\mathrm{i}\omega} \left. \frac{\partial \phi(x, y)}{\partial y} \right|_{y=H}, \tag{3.4}$$

and where

Downloaded from rsta.royalsocietypublishing.org

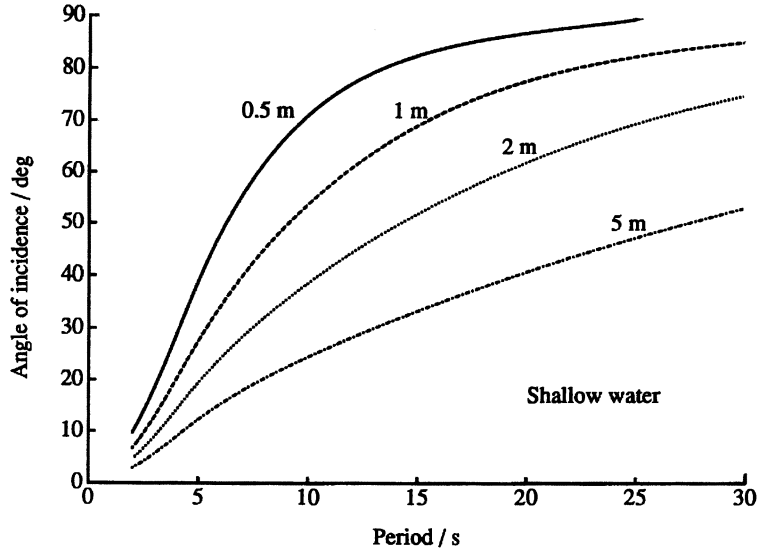

Figure 5. Equivalent curves to figure 3 for shallow water (10 m).

$$\phi(x,y) = \begin{cases} \phi_{\mathrm{o}}(x,y) & x < 0, \\ \phi_{\mathrm{i}}(x,y) & x \geqslant 0. \end{cases} \tag{3.5}$$

Using the mode representation of the potential in equation (2.18) the displacement of the ocean's free surface is given by

$$\mathrm{i}\omega\zeta_{\mathrm{o}}(x) = \left(I\mathrm{e}^{-\mathrm{i}k'_{\mathrm{T}}x} + R\mathrm{e}^{\mathrm{i}k'_{\mathrm{T}}x}\right) k_{\mathrm{T}} \sinh k_{\mathrm{T}}H - \sum_{n=1}^{\infty} a_n k_n \mathrm{e}^{k'_n x} \sin k_n H. \tag{3.6}$$

Similarly the displacement of the ice sheet from equilibrium is given by

$$\begin{aligned}\mathrm{i}\omega\zeta_{\mathrm{i}} = {} & T\mathrm{e}^{-\mathrm{i}\kappa'_{\mathrm{T}}x}\kappa_{\mathrm{T}} \sinh \kappa_{\mathrm{T}}H - b_+\kappa_{\mathrm{D}}\mathrm{e}^{-\kappa'_{\mathrm{D}}x} \sin \kappa_{\mathrm{D}}H - b_-\kappa^*_{\mathrm{D}}\mathrm{e}^{-\kappa'^*_{\mathrm{D}}x} \sin \kappa^*_{\mathrm{D}}H \\ & - \sum_{n=1}^{\infty} b_n \kappa_n \mathrm{e}^{-\kappa'_n x} \sin \kappa_n H. \end{aligned} \tag{3.7}$$

(e) *Strain in the ice sheet*

The strain at the surface of the ice sheet at a point (x, z) where $x > 0$, and in a direction θ to the x axis, is the fractional extension of the ice in that direction. When the displacement is small the strain $s(x, z, \theta)$ is related to the local radius of curvature of the ice sheet in the vertical plane at angle θ, denoted $r(x, z, \theta)$, by

$$\begin{aligned} s(x,z,\theta) &= -\tfrac{1}{2}h\frac{1}{r(x,z,\theta)} \\ &= -\tfrac{1}{2}h(\cos\theta \quad \sin\theta) \begin{pmatrix} \dfrac{\partial^2\eta}{\partial x^2} & \dfrac{\partial^2\eta}{\partial x \partial z} \\ \dfrac{\partial^2\eta}{\partial x \partial z} & \dfrac{\partial^2\eta}{\partial z^2} \end{pmatrix} \begin{pmatrix} \cos\theta \\ \sin\theta \end{pmatrix} \end{aligned} \tag{3.8}$$

Downloaded from rsta.royalsocietypublishing.org

At each instant in time and at each point, the principal strains ϵ are given by the eigenvalues of the matrix

$$\epsilon = -\tfrac{1}{2}h \begin{pmatrix} \dfrac{\partial^2\eta}{\partial x^2} & \dfrac{\partial^2\eta}{\partial x \partial z} \\ \dfrac{\partial^2\eta}{\partial x \partial z} & \dfrac{\partial^2\eta}{\partial z^2} \end{pmatrix}, \tag{3.9}$$

and the directions of the principal strains are given by its eigenvectors. The directions of the principal strains can be shown to satisfy (Timoshenko & Woinowsky-Krieger 1970)

$$\tan(2\theta) = 2\frac{\partial^2\eta}{\partial x \partial z} \Big/ \left(\frac{\partial^2\eta}{\partial x^2} - \frac{\partial^2\eta}{\partial z^2}\right). \tag{3.10}$$

Since the physical displacement is

$$\eta(x, z, t) = \mathrm{Re}\,(\zeta(x))\cos(\omega t + k_z z) - \mathrm{Im}\,(\zeta(x))\sin(\omega t + k_z z), \tag{3.11}$$

writing $\varphi = \omega t + k_z z$ the strain tensor ϵ becomes

$$\begin{aligned} \epsilon = &-\tfrac{1}{2}h\cos\varphi \begin{pmatrix} \mathrm{Re}\left(\dfrac{\partial^2\zeta_\mathrm{i}}{\partial x^2}\right) & -k_z\mathrm{Im}\left(\dfrac{\partial\zeta_\mathrm{i}}{\partial x}\right) \\ -k_z\mathrm{Im}\left(\dfrac{\partial\zeta_\mathrm{i}}{\partial x}\right) & -k_z^2\mathrm{Re}\,(\zeta_\mathrm{i}) \end{pmatrix} \\ &+\tfrac{1}{2}h\sin\varphi \begin{pmatrix} \mathrm{Im}\left(\dfrac{\partial^2\zeta_\mathrm{i}}{\partial x^2}\right) & -k_z\mathrm{Re}\left(\dfrac{\partial\eta}{\partial x}\right) \\ -k_z\mathrm{Re}\left(\dfrac{\partial\eta}{\partial x}\right) & -k_z^2\mathrm{Im}\,(\zeta_\mathrm{i}) \end{pmatrix}. \end{aligned} \tag{3.12}$$

At each point in the ice sheet the maximum principal strain, which coincides with the maximum strain occuring at the point, can be found as the largest eigenvalue of ϵ in equation (3.12) as φ ranges from 0 to 2π.

4. Results

(*a*) *Reflexion and transmission plots*

In figures 6, 7 and 8 we have plotted for three ice thicknesses respectively, the amplitude reflexion coefficient as a function of incidence angle at wave periods 5 s, 10 s, and 20 s, and the corresponding transmission coefficient curves in this case with respect to angle of transmission. The plots are drawn perpendicular to one another to enable the reader to relate angle of incidence to angle of transmission using the additional plot provided.

The reflexion coefficient curves of figures 6, 7 and 8 are all similar in structure. In most cases the reflexion coefficient decreases from its value at normal incidence to a minimum, and then increases rapidly to unity at the critical angle. The 20 s case is slightly different in figures 6 and 7 which correspond to relatively thin ice for a wave of this wavelength. Here the wave is long enough to suffer minimal reflexion at the ice edge, and the reflexion coefficient subsequently increases monotonically as angle of incidence is increased, reaching a value of one only at grazing incidence.

The plots of incidence angle θ_o versus transmission angle θ_i are also similar

PHILOSOPHICAL TRANSACTIONS OF THE ROYAL SOCIETY A MATHEMATICAL, PHYSICAL & ENGINEERING SCIENCES
PHILOSOPHICAL TRANSACTIONS OF THE ROYAL SOCIETY A MATHEMATICAL, PHYSICAL & ENGINEERING SCIENCES

Downloaded from rsta.royalsocietypublishing.org

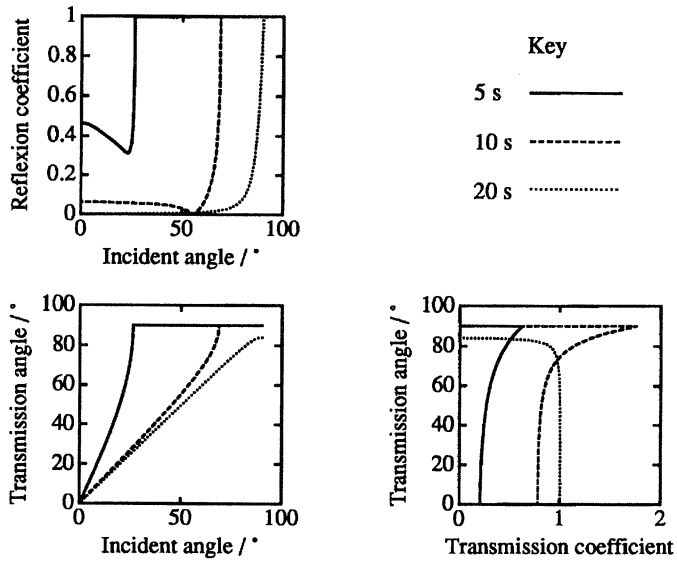

Figure 6. The reflexion coefficient plotted as a function of angle of incidence, the transmission coefficient plotted as a function of angle of transmission, and the relationship between the angles of incidence and transmission for 1 m thick sea ice on 100 m of water.

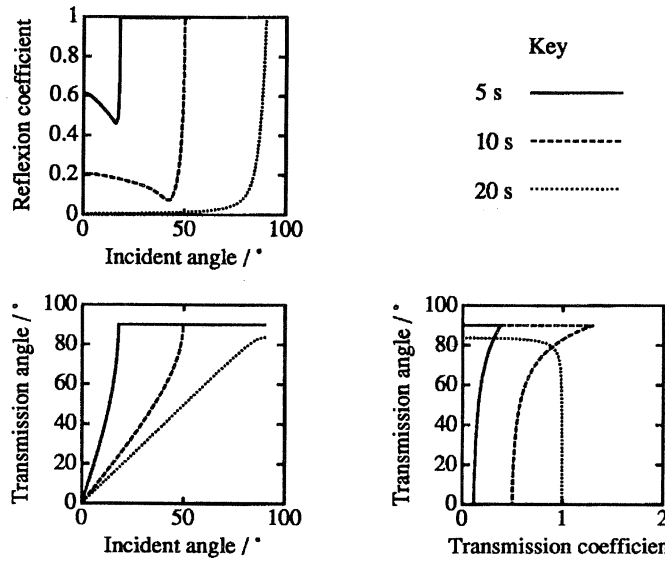

Figure 7. Equivalent curves to figure 6 for ice of 2 m thickness.

at each thickness. Again in most cases $\theta_i > \theta_o$, with θ_i attaining 90° at some critical angle of incidence in the range $0 < \theta_o < 90°$. The 0–critical angle range of incidence angles is therefore mapped onto a 0–90° range of transmission angles. The two 20 s curves in figures 6 and 7 again behave differently. For most incidence angles $\theta_i \approx \theta_o$. However, as the wave nears grazing incidence, i.e. $\theta_o \to 90°$, the value of θ_i drops below θ_o. This is caused by the effect discussed in § 3 *b*; the model degenerates to a mass-loading model at these wave numbers.

Excluding the 20 s wave in figures 6 and 7, the transmission angle increases

Downloaded from rsta.royalsocietypublishing.org

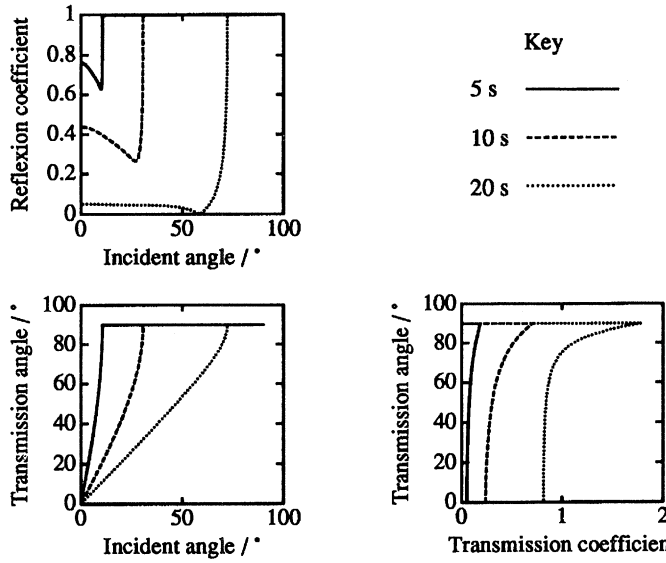

Figure 8. Equivalent curves to figure 6 for ice of 5 m thickness.

from its value at normal incidence to a maximum at the critical incidence angle. Thereafter transmission decreases to zero at grazing incidence. The transmission angles for 20 s waves at ice thicknesses of 1 m and 2 m, however, essentially remain at their normal incidence values of one before gradually decreasing monotonically, reaching zero at grazing incidence.

The effect of increasing wave period on the reflexion coefficient is to move the respective curves towards higher incidence angles, i.e. long waves are less likely to be totally reflected from the ice sheet than are short waves. The effect of increasing thickness is to move the curves towards lower incidence angles, i.e. as would be expected, thick ice is more likely to totally reflect incoming waves. Long wave periods in thin ice, as we have seen above, do not have critical angles in the $0 < \theta_o < 90°$ range; their 'critical angle' occurs at grazing incidence, i.e. when $\theta_o = 90°$.

(*b*) *Three-dimensional plots*

Figures 9 and 10 illustrate the behaviour of the reflexion coefficient as a function of both incidence angle and wave period. The three-dimensional plots are for 1 m thick sea ice, at a water depth of 100 m and 10 m respectively. In each case the variation with the period is drawn as a solid curve, and the variation with incidence angle is drawn dashed. The critical angle is reached when the solid curves reach a reflexion coefficient of unity and the concomitant critical angle curve is shown dotted. There is a distinct difference between the structure of the curves for the 100 m (intermediate depth) and 10 m (shallow depth) cases, whereas the equivalent deep water (1000 m) curves are very similar to those of figure 9 and have therefore not been included. The differences shown reflect the structure of the corresponding curves of figures 6–8, and the critical angle plots of figures 3–5.

Downloaded from rsta.royalsocietypublishing.org

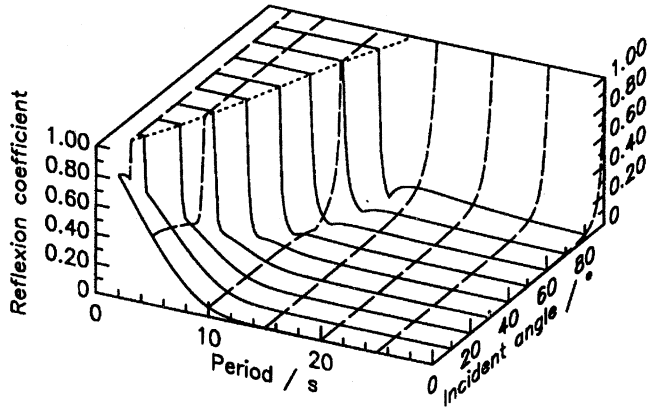

Figure 9. Three-dimensional plot showing the variation of reflexion coefficient with angle of incidence and wave period for 1 m thick sea ice on a water depth of 100 m. The critical angle curve corresponding to figure 4 is shown dotted.

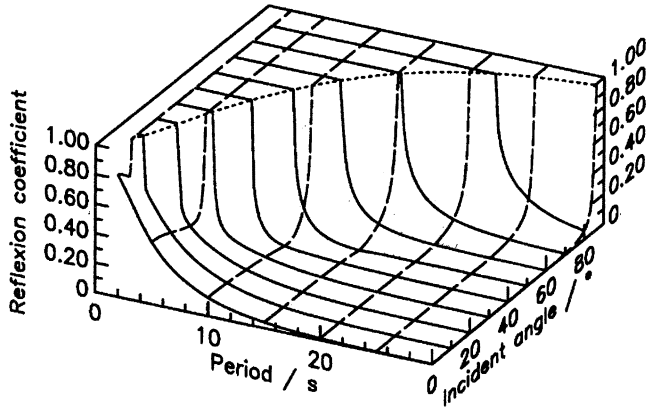

Figure 10. Equivalent curves to figure 9 for a water depth of 10 m. The critical angle curve corresponding to figure 5 is shown dotted.

(*c*) *Strain*

In this section we present some results which derive from expressions (3.9) and (3.12) of § 3 *e* as a series of figures 11–17 intended to illustrate the various possibilities that can arise when a wave train of a given period propagates into shore fast sea ice. Three angles of incidence are considered: 0°, 30°, and 60°; and three periods: 5 s, 10 s and 20 s. Results are given only for a single water depth of 100 m and a single ice thickness of 1 m; equivalent graphs may of course be computed for any realistic water depth or ice thickness. All curves are normalized to 1 m incident wave amplitude. Each figure in the series comprises three parts: an upper part where the strain in the x-direction, i.e. perpendicular to the ice edge, is plotted as a function of distance from the ice edge; a lower part where the maximum absolute principal strain is plotted, again with distance from the ice edge; and a middle part where directed line segments are plotted representing the two principal strains and their directions through the wave cycle, with the convention that positive strain is drawn solid and negative strain is drawn dotted.

Downloaded from rsta.royalsocietypublishing.org

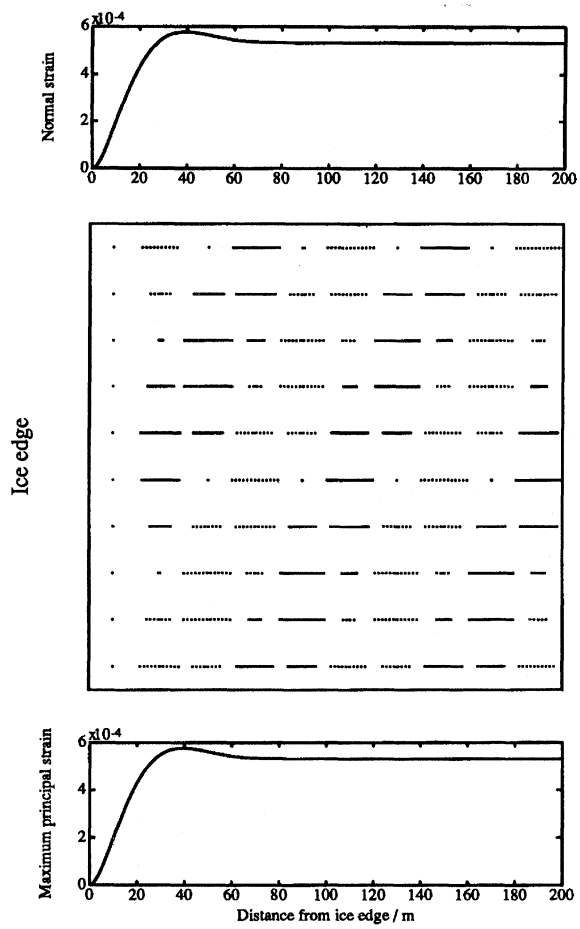

Figure 11. Strain normal to the ice edge as a function of penetration (upper figure), schematic showing principal strains propagating into the ice cover with positive strain drawn solid and negative strain drawn dotted (middle figure), and maximum principal strain as a function of penetration (lower figure). In this case the waves are of 5 s period and are normally incident onto a 1 m thick ice sheet floating on 100 m of water.

The middle schematic, therefore, has distance from the ice edge across the page as usual, and time perpendicular to this. In all cases we show results for only the outer 200 m of the ice sheet.

Figure 11 is for waves with 5 s period entering the ice sheet at normal incidence. As such it may be compared directly with fig. 3*a* of Fox & Squire (1991*a*). Since the wave is propagating in the x-direction the model reduces to two-dimensions, and boundary conditions (2.8) and (2.9) at the ice edge become simply

$$\frac{\partial^2}{\partial x^2}\left(\frac{\partial \phi}{\partial y}\right) = \frac{\partial^3}{\partial x^3}\left(\frac{\partial \phi}{\partial y}\right) = 0, \qquad x = 0^+, \quad y = H. \tag{4.1}$$

The maximum principal strain in this case is just the strain perpendicular to the ice edge, so that the upper and lower figures are identical; the second principal strain vanishes. Furthermore, the simplified boundary conditions (4.1) impose the

Downloaded from rsta.royalsocietypublishing.org

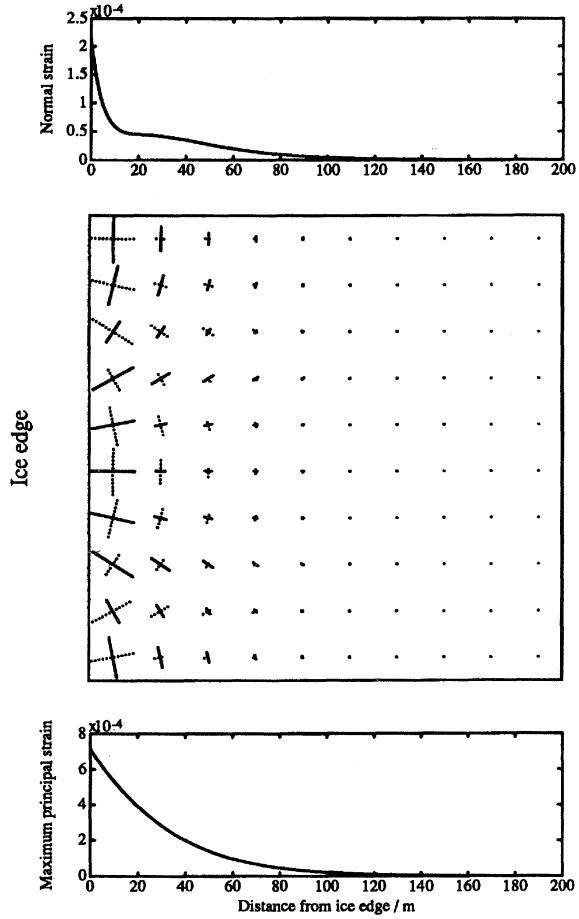

Figure 12. Equivalent strain plots to figure 11 for an angle of incidence of 30°.

constraint that the bending moment – and hence the strain – must vanish at the ice edge itself, together with its x-derivative. From its zero ice edge value figure 11 shows that the strain resulting from an incoming wave of unit amplitude rises rapidly to a value which is large enough to cause the ice sheet to break. (Sea ice has been observed to fracture at a strain of 3×10^{-5} by Goodman *et al.* (1980), and between 4.4×10^{-5} and 8.5×10^{-5} by Squire & Martin (1980).) In the far-field the curve approaches an asymptote as the strains due to evanescent and damped-travelling wave modes die away to leave only the transmitted wave component. The equivalent figures for 10 s and 20 s period waves have almost identical shape, differing only in the wavelength of the transmitted wave in the ice sheet and also in the position of maximum strain; the maximum strain occuring at 60 m and 65 m from the ice edge for 10 s and 20 s period waves respectively. The far-field strain magnitude is strongly dependent on wave period (and also ice thickness) and drops from close to 6×10^{-4} at 5 s period to close to 5.5×10^{-4} at 10 s and to 8×10^{-5} for 20 s period waves; the ice bends most easily within a band of periods determined by both the reflexion/transmission process and curvature which act in opposition. At short periods (or for thick ice) the strain reaches a maximum

Downloaded from rsta.royalsocietypublishing.org

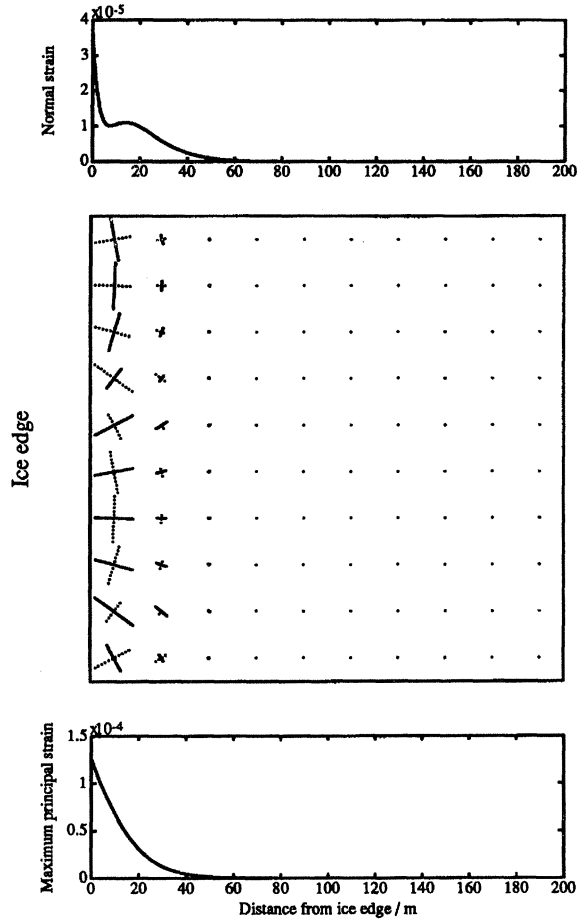

Figure 13. Equivalent strain plots to figure 11 for an angle of incidence of 60°.

before dropping to its asymptotic limit, but as the period increases the peak becomes less pronounced and for long periods the strain increases monotonically from zero at the ice edge to its interior asymptotic value.

In figures 12, 14 and 16 equivalent results to the above are shown when the angle of incidence $\theta_o = 30°$. In this case the strain normal to the ice edge and the maximum principal strain are not identical, as the waves no longer propagate in the x-direction. The second principal strain is now non-zero. Also consequent to the boundary conditions (2.8) and (2.9), strain does not vanish at the ice edge. The 5 s result of figure 12 is perhaps the most interesting as in this case a glance at figure 4 shows the incoming wave to be supercritical, i.e. no travelling wave mode penetrates the ice cover and the effect of the incoming wave is manifested purely as the sum of evanescent modes which decay away from the ice edge. Both the strain normal to the ice edge (upper figure) and the maximum principal strain (lower figure) decrease monotonically from their values at $x = 0$ to zero, though the former strain shows some fine structure. By about 100 m there is no significant strain. In figures 14 and 16 equivalent results are presented for 10 s and 20 s waves

Downloaded from rsta.royalsocietypublishing.org

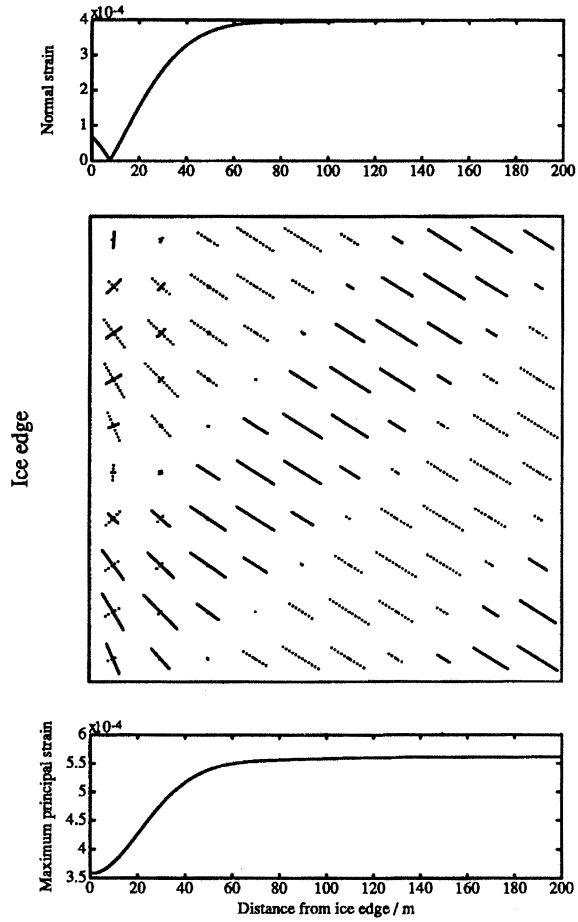

Figure 14. Strain normal to the ice edge as a function of penetration (upper figure), schematic showing principal strains propagating into the ice cover with positive strain drawn solid and negative strain drawn dotted (middle figure), and maximum principal strain as a function of penetration (lower figure). In this case the waves are of 10 s period and are incident onto a 1 m thick ice sheet floating on 100 m of water with an angle of incidence of 30°.

respectively. In both cases the wave is incident on the ice sheet at a subcritical angle of incidence θ_o, so a travelling wave is generated within the ice to which the strain field settles down in the far-field. The travelling wave propagates at an angle θ_i to the x-axis. Closer to the ice edge, where the evanescent and damped-travelling modes still play a role, the situation is quite confused as can be seen in the middle schematic of each figure. Indeed the strain normal to the ice edge decreases from its ice edge value to a minimum some 8 m in, before then increasing monotonically to its far-field magnitude. The maximum principal strain increases steadily from its ice edge value up to its interior value.

Results for $\theta_o = 60°$, as shown in figures 13, 15 and 17, are similar to those when $\theta_o = 30°$. The 5 s wave case shown in figure 13 again impinges on the ice plate supercritically, but in this case the fine structure evident in the upper figure representing the magnitude of the strain perpendicular to the ice edge is

Downloaded from rsta.royalsocietypublishing.org

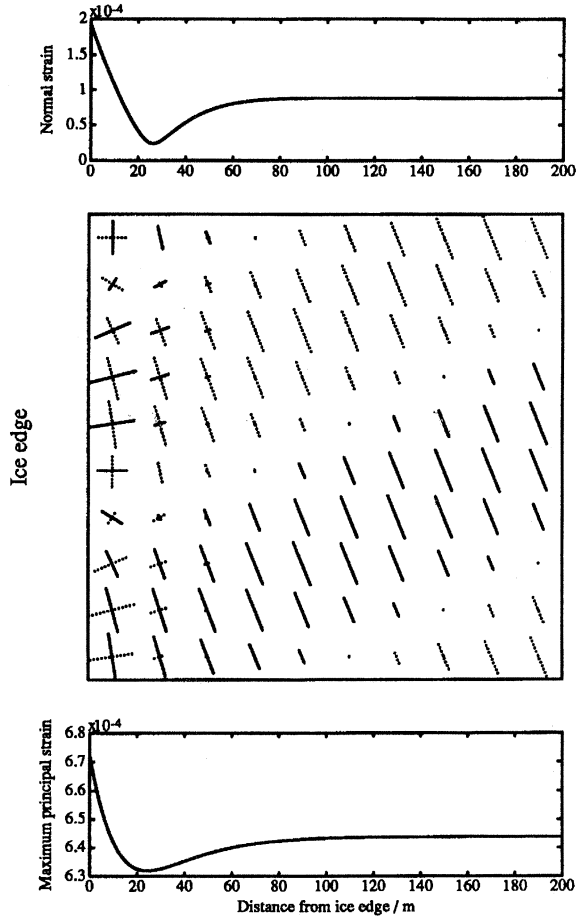

Figure 15. Equivalent strain plots to figure 14 for an angle of incidence of 60°.

more pronounced. Here a peak strain is predicted at about 16 m penetration. Subsequently – like the maximum principal strain – the strain decreases to zero, becoming insignificant at about 60 m where the evanescent modes have attenuated. Figures 15 and 17, showing 10 s and 20 s waves entering at 60° incidence, are again subcritical examples so in both cases a transmitted wave exists for large x. Hence both the maximum principal strain and the normal strain tend asymptotically to a non-zero value in the far-field. Again, closer to the ice edge the strain field is complicated due to the presence of evanescent and damped-travelling modes.

(*d*) *Energy density*

At a single frequency the infinitesimal incident energy density $\mathrm{d}E_\mathrm{o}$ associated with an infinitesimal angular spread $\mathrm{d}\theta_\mathrm{o}$ is given by

$$\mathrm{d}E_\mathrm{o} = G_\mathrm{o}(\theta_\mathrm{o})\,\mathrm{d}\theta_\mathrm{o}, \tag{4.2}$$

where $G_\mathrm{o}(\theta_\mathrm{o})$ is the incident energy density per angle of incidence, which is also known as the (open water) spreading function. Denoting the amplitude far-field

Downloaded from rsta.royalsocietypublishing.org

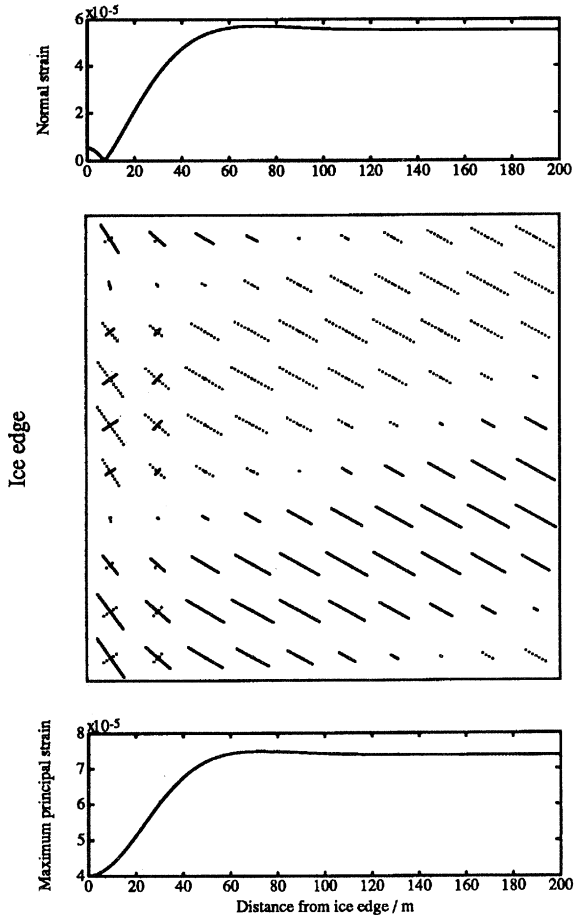

Figure 16. Strain normal to the ice edge as a function of penetration (upper figure), schematic showing principal strains propagating into the ice cover with positive strain drawn solid and negative strain drawn dotted (middle figure), and maximum principal strain as a function of penetration (lower figure). In this case the waves are of 20 s period and are incident onto a 1 m thick ice sheet floating on 100 m of water with an angle of incidence of 30°.

transmission coefficient at angle θ_o by $\mathcal{T}$, the energy in the corresponding infinitesimal range of transmitted angles $d\theta_i$ is

$$dE_i = \mathcal{T}^2\, dE_o = G_i(\theta_i)\, d\theta_i, \tag{4.3}$$

where $G_i(\theta_i)$ is the spreading function in the ice-covered region (the energy density per angle of transmission). Hence,

$$G_i(\theta_i) = \mathcal{T}^2 G_o(\theta_o) \frac{d\theta_o}{d\theta_i}. \tag{4.4}$$

We first consider an omnidirectional sea, i.e. one where $G_o(\theta_o) \equiv 1$. Then the spreading function in the ice is simply

$$G_i(\theta_i) = \mathcal{T}^2 \frac{d\theta_o}{d\theta_i}. \tag{4.5}$$

Downloaded from rsta.royalsocietypublishing.org

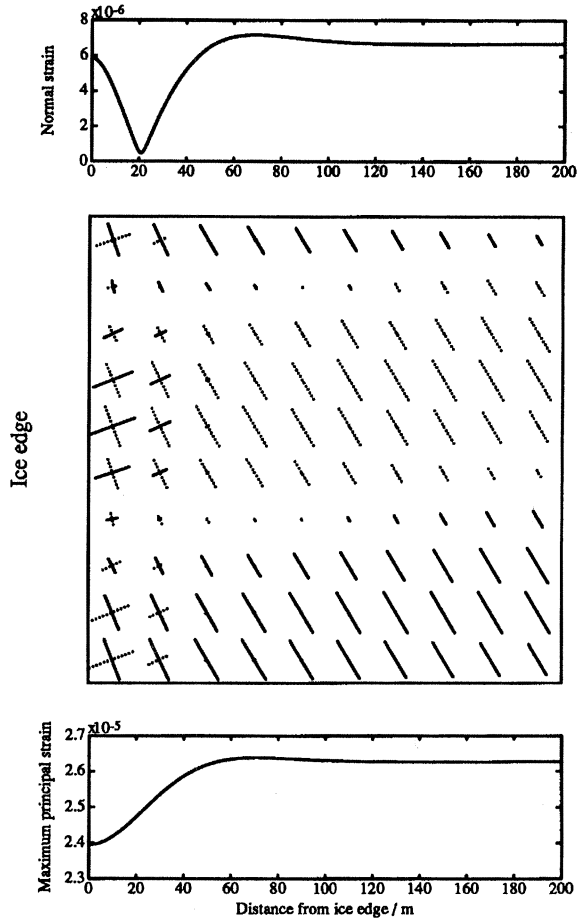

Figure 17. Equivalent strain plots to figure 16 for an angle of incidence of 60°.

The function $G_i(\theta_i)$ is plotted in figure 18 for several wave periods and ice thicknesses. All curves are symmetric about normal incidence/transmission. At 10 s and 20 s in a 1 m ice sheet, $G_i(\theta_i)$ is relatively insensitive to transmission angle θ_i, except near critical incidence where the curves decrease rapidly to zero. Here the transmitted wave is propagating almost parallel to the ice edge. The curves also drop to zero in the situation where no critical angle exists, but only at grazing incidence where the transmission coefficient vanishes. At 5 s the curve begins to show some structure, with a minimum forming at normal transmission, and two maxima forming at a transmission angle of about 63°. A 5 s wave suffers considerable reflexion at the ice edge so $G_i(\theta_i)$ for this period takes on rather small values. For convenience the same 5 s curve is also shown solid in the right hand figure, where the effect of thickness is considered. Here it is clear that an increase in thickness serves mainly to diminish the amount of energy penetrating the sea ice, the curves have roughly the same qualitative form, though there is a slight movement of the peak towards higher incidence angles (2 m: $\sim 66°$, 5 m: $\sim 69°$).

We now relax our omnidirectional condition and consider a sea with a unimodal structure. After Longuet-Higgins *et al.* (1963) the open water spreading function

Downloaded from rsta.royalsocietypublishing.org

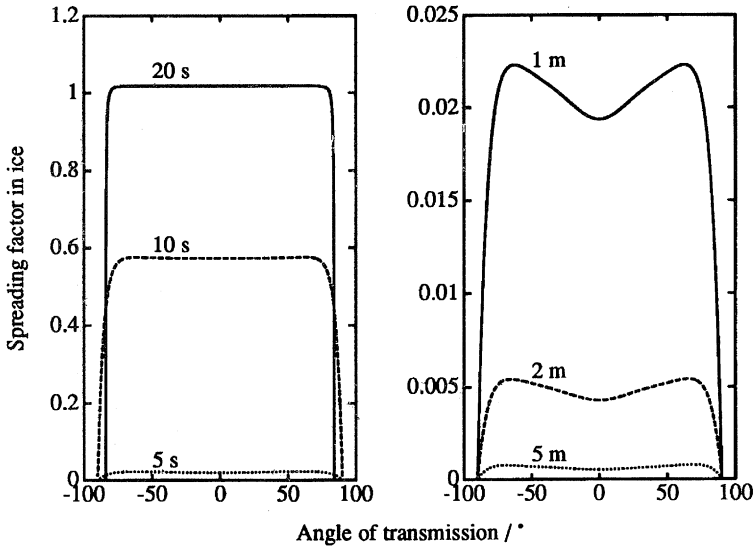

Figure 18. The ice spreading function $G_i(\theta_i)$ for a water depth of 100 m. The figure on the left shows $G_i(\theta_i)$ for 5 s, 10 s and 20 s wave periods in 1 m of sea ice; the figure on the right shows $G_i(\theta_i)$ for 1 m, 2 m and 5 m of ice at a wave period of 5 s.

$G_o(\theta_o)$, about a principal wave direction $\overline{\theta_o}$, is then assumed to take the form

$$G_o(\theta_o) = \cos^{2s}(\tfrac{1}{2}(\theta_o - \overline{\theta_o})). \tag{4.6}$$

The factor s is strictly a frequency dependent index. Indeed Hasselmann *et al.* (1980) suggests that $s = 9.77(f/f_m)^{-2.33}$, where f_m is the frequency corresponding to the peak in the power spectral density. The root mean square spread about the mean wave direction is therefore a function of wave period. For the present study we have taken $s = 10$ after Ewing & Laing (1987), who found this to be typical of their measured values close to the spectral peak for seas near full development. The drop off with frequency predicted by Hasselmann and co-workers is greater than observed by Ewing *et al.* (1987). In the present context, the neglect of any frequency dependence in the spreading function $G_o(\theta_o)$ is not seen as critical, as changing s does not alter the final result markedly. A value of $s = 10$ implies a root mean square spread of approximately 24°.

Using expression (4.6), an energy density value corresponding to a single principal angle of incidence may be found by integrating equation (4.2) over all admissible angles. We consider only the energy impinging on the ice sheet in this calculation, i.e. we do not include waves travelling away from the ice in our integration. In a similar way, equation (4.3) may also be integrated – substituting for $G_i(\theta_i)$ from equation (4.4) – to give a single value for the energy density inside the ice cover corresponding to the same principal incidence angle. We now allow the principal angle of incidence to range from −90° to 90°, thereby defining two energy density curves; one for the open water energy incident on the ice sheet, and one for the transmitted energy in the ice sheet in the far-field. Open water curves (drawn solid) are plotted as functions of principal incidence angle $\overline{\theta_o}$ in figures 19, 20 and 21. The figures correspond to the same 1 m ice thickness, but are respectively for 5 s, 10 s and 20 s period waves. Also plotted (drawn dashed)

Downloaded from rsta.royalsocietypublishing.org

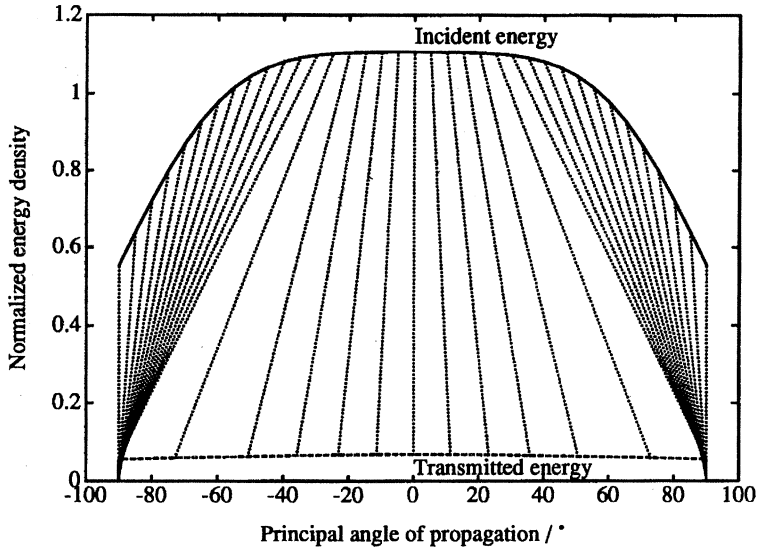

Figure 19. The incident normalized energy density (solid line) and the transmitted far-field energy density (dashed line) for a 5 s wave for various principal angles of propagation. Ice thickness is 1 m and water depth is 100 m. The dotted lines joining the two curves show the mapping between the angle of incidence and the angle of transmission. For discussion see text.

are the equivalent curves within the ice cover plotted against the mean angle of transmission $\overline{\theta_i}$, say, corresponding to $\overline{\theta_o}$. The mapping between $\overline{\theta_o}$ and $\overline{\theta_i}$ is shown by the dotted lines linking the curves in each figures. All incident energies are normalized to unit amplitude waves. At 5 s (figure 19) the energy density within the ice at all mean angles of incidence is markedly reduced due to the reflexion process at the edge. In this case the maximum energy density in the ice occurs at normal incidence. A rather different picture emerges for 10 s wave (figure 20), where less reflexion takes place at the ice edge with the result that more energy is available in the far-field. Here the peak energy density does not occur at normal incidence, but at an angle of transmission of about 55°. In figure 21, where a 20 s wave is considered, minimal reflexion occurs at the edge of the 1 m ice sheet and the two energy density curves almost superimpose. Energy density is maximum for waves propagating with their mean direction normal to the ice edge. Unlike the previous two figures, figure 21 represents a situation where no critical angle exists and thus $\theta_i \leqslant \theta_o$.

5. Conclusions

In this paper we have developed a precise linearized model for the reflexion/transmission process at the margin of a sheet of shore fast sea ice, and we have then gone on to report some of the model's predictions. The model has two shortcomings which the reader might question: the use of linearized equations; and the use of a small deformation-gradient elastic constitutive relation for sea ice. The former assumption has been addressed in a recent paper dealing with normal incidence by Fox (1992), which investigates the consequences of including second order terms in the equations. The higher order work shows the develop-

PHILOSOPHICAL TRANSACTIONS OF THE ROYAL SOCIETY A MATHEMATICAL, PHYSICAL & ENGINEERING SCIENCES
PHILOSOPHICAL TRANSACTIONS OF THE ROYAL SOCIETY A MATHEMATICAL, PHYSICAL & ENGINEERING SCIENCES

Downloaded from rsta.royalsocietypublishing.org

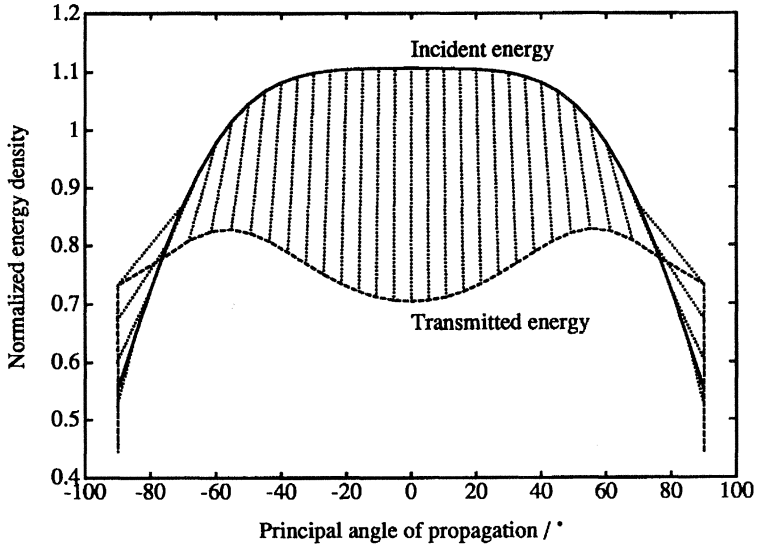

Figure 20. Equivalent curves to figure 19 for a wave period of 10 s.

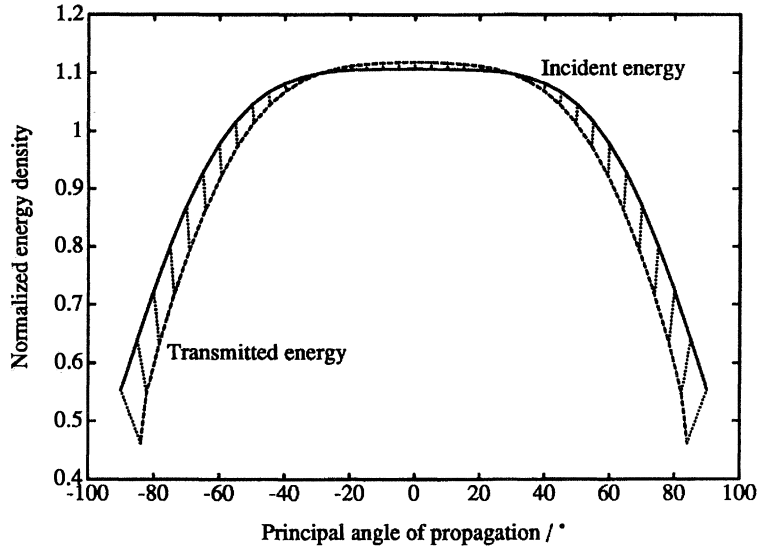

Figure 21. Equivalent curves to figure 19 for a wave period of 20 s.

ment presented here to be valid over a wide range of incident wave amplitude conditions. The adoption of a linear elastic theory, again at normal incidence, is relaxed in Squire & Fox (1992) where some viscosity is included in the plate boundary condition (2.7). Its principal effect is to impose attenuation on the travelling wave, and this gradual decay is actually seen in the few observations that are available (Squire & Fox 1992). These data support a linear viscoelastic formulation with a small, velocity-dependent damping term in the plate equation, though too few measurements are available to be sure of its magnitude for different ice types. The inclusion of viscosity does not change significantly any

Downloaded from rsta.royalsocietypublishing.org

of the results reported in the current paper if the travelling wave is assumed to decay gradually with distance from the ice margin.

Results from this work are not limited solely to the interaction of ocean waves with sheets of shore fast sea ice; they have wider appeal. Recently the elastic plate analogy has been used to represent wave propagation into pack ice (Liu & Mollo-Christensen 1988; Liu *et al.* 1991*a*,*b*, 1992; Squire & Fox 1991), and in a simpler form – i.e. with flexural rigidity $L = 0$ – it has been used to represent waves in frazil or pancake ice (Wadhams & Holt 1991). The current paper reports results which have direct application to these studies: it provides the precise behaviour of several relevant parameters, e.g. $\mathcal{R}$, $\mathcal{T}$, the mapping between θ_o and θ_i, the ice spreading function $G_i(\theta_i)$, etc.; and it explains quantitatively features occurring in the various datasets that currently exist or are coming on line with the advent of the ERS-1 synthetic aperture radar datastream.

Significant results in this paper include the following.

1. The precise solution of the wave–ice-interaction problem for shore fast sea ice; results are also pertinent to ocean waves travelling into other ice types such as frazil and pancake ice if $L = 0$, or a marginal ice zone ($L \neq 0$).

2. Critical angle curves for various water depths at a variety of typical ice thicknesses (figures 3–5).

3. Reflexion and transmission coefficient curves at different periods, and the mapping between angle of incidence θ_o and angle of transmission θ_i (figures 6–8).

4. Principal strain curves and strains normal to the ice edge for various angles of incidence and wave period (figures 11–17).

5. The spreading function $G_i(\theta_i)$, computed for an omnidirectional incident sea (figure 18).

6. Normalized energy densities as a function of incidence angle using an open water spreading function described by equation (4.6) for various wave periods (figures 19–21).

The authors are indebted to the New Zealand Foundation for Research, Science and Technology, the Universities of Otago and Auckland, the New Zealand University Grants Committee, and the New Zealand Department of Scientific and Industrial Research for their support. The majority of the numerical work in this paper was carried out using the MATLAB^{TM} computer language; its abilities are acknowledged without reserve.

Appendix A. The ice edge boundary conditions

Suppose $X = (0, x_1)$ and $Z = (z_0, z_1)$ are intervals in the plane of the plate, and let $T = (t_0, t_1)$ be an interval in time. A variational statement of equation (2.6) can be formed by multiplying both sides of the differential equation by a variation $\delta\eta$ and integrating the result over the region $X \times Z \times T$. Writing $p = P_i - mg$

PHILOSOPHICAL TRANSACTIONS OF THE ROYAL SOCIETY A MATHEMATICAL, PHYSICAL & ENGINEERING SCIENCES

PHILOSOPHICAL TRANSACTIONS OF THE ROYAL SOCIETY A MATHEMATICAL, PHYSICAL & ENGINEERING SCIENCES

Downloaded from rsta.royalsocietypublishing.org

and using suitable transformations (Hildebrand 1965) we find that

$$\begin{aligned}\delta \iiint_{X\times Z\times T} & \left(L\{\tfrac{1}{2}(\eta_{xx}^2+\eta_{zz}^2+(1-\alpha)\eta_{xz}^2+\alpha\eta_{xx}\eta_{zz}\}-\tfrac{1}{2}m\eta_t^2-p\eta\right)\mathrm{d}x\,\mathrm{d}z\,\mathrm{d}t \\ &+\iint_{X\times Z} m\left[\eta_t\delta\eta\right]_{t_0}^{t_1}\mathrm{d}x\;\mathrm{d}z \\ &+\iint_{Z\times T}\left[\left(L\frac{\partial\nabla_{xz}^2\eta}{\partial x}+(1-\alpha)L\eta_{xzz}\right)\delta\eta-L\left(\eta_{xx}+\alpha\eta_{zz}\right)\delta\eta_x\right]_0^{x_1}\mathrm{d}z\,\mathrm{d}t \\ &+\iint_{X\times T}\left[\left(L\frac{\partial\nabla_{xz}^2\eta}{\partial z}+(1-\alpha)L\eta_{xxz}\right)\delta\eta-L\left(\eta_{zz}+\alpha\eta_{xx}\right)\delta\eta_z\right]_{z_0}^{z_1}\mathrm{d}x\,\mathrm{d}t \\ &-\int_T\left[\left[2L(1-\alpha)\eta_{xz}\delta\eta\right]_0^{x_1}\right]_{z_0}^{z_1}\mathrm{d}t \\ &=0 \end{aligned} \tag{A 1}$$

for any constant α. In this problem the terms in each integrand have physical significance when α is identified with the Poisson's ratio, ν, for sea ice.

In the first integral the part of the integrand involving L is the strain energy due to the curvature of the plate, the term $-p\eta$ is the potential energy due to the transverse pressure, and $\frac{1}{2}m\eta_t^2$ is the kinetic energy, all per unit area. Each of these terms give instantaneous energies. In the third integral the term multiplying the variation at the ice edge, $\delta\eta$ at $x=0$, is minus the effective transverse force associated with the variation in deflexion, while the term multiplying the variation in normal derivative $\delta\eta_x$ is the associated bending moment. Terms in the fourth integral have similar interpretations along the lines $z=$ const..

The first line of equation (A 1) is the variation of an integral over the whole region, whereas the subsequent boundary integrals depend only on η, its variation $\delta\eta$, and their derivatives on the boundary of the space-time region $X\times Z\times T$. The *natural* boundary conditions at the ice edge, corresponding to the fact that it is free to move, are found by ensuring that the contributions to the boundary integrals when $x=0$ are each zero. Consequently we need only consider the boundary conditions required to make the $x=0$ term in the third integral vanish. This occurs when there is no net transverse force or bending moment at the ice edge $x=0^+$, i.e, when

$$L\frac{\partial}{\partial x}\nabla_{xz}^2\eta+(1-\nu)L\eta_{xzz}=0, \tag{A 2}$$

and

$$L\left(\eta_{xx}+\nu\eta_{zz}\right)=0. \tag{A 3}$$

References

Bates, H. F. & Shapiro, L. H. 1980 Long-period gravity waves in ice-covered sea. *J. geophys. Res.* **85**, 1095–1100.

Evans, D. V. & Davies, T. V. 1968 *Wave–ice interaction.* New Jersey: Davidson Lab., Stevens Inst. of Technol., Rep. 1313.

Ewing, J. A. & Laing, A. K. 1987 Directional spectra of seas near full development. *J. phys. Oceanogr.* **17**, 1696–1706.

PHILOSOPHICAL TRANSACTIONS OF THE ROYAL SOCIETY A MATHEMATICAL, PHYSICAL & ENGINEERING SCIENCES

PHILOSOPHICAL TRANSACTIONS OF THE ROYAL SOCIETY A MATHEMATICAL, PHYSICAL & ENGINEERING SCIENCES

Downloaded from rsta.royalsocietypublishing.org

Ewing, M. & Crary, A. P. 1934 Propagation of elastic waves in ice. II. *Physics* **5**, 181–184.

Ewing, M., Crary, A. P. & Thorne, A. M. 1934 Propagation of elastic waves in ice. I. *Physics* **5**, 165–168.

Forbes, L. K. 1986 Surface waves of large amplitude beneath an elastic sheet. 1. High-order series solution. *J. Fluid Mech.* **169**, 409–428.

Forbes, L. K. 1988 Surface waves of large amplitude beneath an elastic sheet. 2. Galerkin solution. *J. Fluid Mech.* **188**, 491–508.

Fox, C. 1992 Large amplitude sea/ice coupling. In *Advances in Ice Technology: Proc. of the Third Int. Conf. on Ice Technology, 11–13 August 1992, Cambridge, MA, USA* (ed. T. K. S. Murthy, W. M. Sackinger & P. Wadhams), pp. 293–304. Computational Mechanics Publications.

Fox, C. & Squire, V. A. 1990 Reflexion and transmission characteristics at the edge of shore fast sea ice. *J. geophys. Res.* **95**, 11629–11639.

Fox, C. & Squire, V. A. 1991*a* Strain in shore fast ice due to incoming ocean waves and swell. *J. geophys. Res.* **67**, 4531–4547.

Fox, C. & Squire, V. A. 1991*b* Coupling between an ocean and an ice shelf. *Annls Glaciol.* **15**, 101–108.

Frankenstein, G. & Garner, R. 1967 Equations for determining the brine volume of sea ice from −0.5 °C to −22.9 °C. *J. Glaciol.* **6**, 943–944.

Gill, P. E., Murray, W. & Wright, M. H. 1981 *Practical optimization,* pp. 144–153. London: Academic Press.

Goodman, D. J., Wadhams, P. & Squire, V. A. 1980 The flexural response of a tabular ice island to ocean swell, *Annls Glaciol.* **1**, 23–27.

Grande, O. H. 1983 Model study of wave propagation in a continuous ice sheet. MSc thesis, Memorial University of Newfoundland.

Green, T. 1985 The natural oscillations of an ice-covered channel. *J. Glaciol.* **30**, 313–320.

Greenhill, A. G. 1887 Wave motion in hydrodynamics. *Am. J. Math.* **9**, 62–112.

Hasselmann, D. E., Barnet, M. & Ewing J. A. 1980 Directional spectra observed during JONSWAP 1973. *J. phys. Oceanogr.* **10**, 1264–1280.

Hendrickson, J. A., & Webb, L. M. 1963 *Theoretical investigation of semi-infinite ice floes in water of infinite depth.* Pasadena, California: Natl. Eng. Sci. Co., Rep. NBy-32225.

Hilderbrand, F. B. 1965 *Methods of applied mathematics,* 2nd edn. Englewood Cliffs: Prentice-Hall.

Keller, J. B. & Goldstein, E. 1953 Water wave reflection due to surface tension and floating ice. *Eos, Wash.* **34**, 43–48.

Keller, J. B. & Weitz, M. 1953 Reflection and transmission coefficients for waves entering or leaving an icefield. *Communs pure appl. Math.* **6**, 415–417.

Kerr, A. D. & Palmer, W. T. 1972 The deformations and stresses in floating ice plates. *Acta mech.* **15**, 57–72.

Liu, A. K. & Mollo-Christensen, E. 1988 Wave propagation in solid ice pack. *J. phys. Oceanogr.* **18**, 1702–1712.

Liu, A. K., Holt, B. & Vachon, P. W. 1991*a* Wave propagation in the marginal ice zone: model predictions and comparisons with buoy and synthetic aperture radar data. *J. geophys. Res.* **96**, 4605–4621.

Liu, A. K., Vachon, P. W. & Peng, C. Y. 1991*b* Observation of wave refraction at an ice edge by synthetic aperture radar. *J. geophys. Res.* **96**, 4803–4808.

Liu, A. K., Vachon, P. W., Peng, C. Y. & Bhogal, A. S. 1992 Wave attenuation in the marginal ice zone during LIMEX. *Atmosphere-Ocean* **30**(2), 192–206.

Longuet-Higgins, M. S., Cartwright, D. E. & Smith, N. D. 1963 Observations of the directional spectrum of sea waves using the motions of a floating buoy. In *Ocean wave spectra*, pp. 111–136. Englewood Cliffs: Prentice-Hall.

Oliver, J., Crary, A. P. & Cotell, R. 1954 Elastic waves in Arctic pack ice. *Eos, Wash.* **35**, 282–292.

PHILOSOPHICAL TRANSACTIONS OF THE ROYAL SOCIETY A MATHEMATICAL, PHYSICAL & ENGINEERING SCIENCES

PHILOSOPHICAL TRANSACTIONS OF THE ROYAL SOCIETY A MATHEMATICAL, PHYSICAL & ENGINEERING SCIENCES

Downloaded from rsta.royalsocietypublishing.org

Peters, A. S. 1950 The effect of a floating mat on water waves. *Communs pure appl. Math.* **3**, 319–354.

Phillips, O. M. 1977 *The dynamics of the upper ocean,* 2nd edn, pp. 139–159. Cambridge University Press.

Press, F. & Ewing, M. 1951 Propagation of elastic waves in a floating ice sheet. *Eos, Wash.* **32**, 673–678.

Press, F., Crary, A. P., Oliver, J. & Katz, S. 1951 Air-coupled flexural waves in floating ice. *Eos, Wash.* **32**, 166–172.

Roethlisberger, H. 1972 Surface waves and waves in thin floating ice. *Cold Reg. Res. Engng Lab. Monogr.* **II-A2a**, 105–109.

Shapiro, A. & Simpson, L. S. 1953 The effect of a broken ice field on water waves. *Eos, Wash.* **34**, 36–42.

Squire, V. A. 1978 Dynamics of ocean waves in a continuous sea ice cover. Ph.D. thesis, University of Cambridge.

Squire, V. A. 1984*a* A theoretical, laboratory and field study of ice-coupled waves. *J. geophys. Res.* **89**, 1079–1089.

Squire, V. A. 1984*b* On the critical angle for waves entering shore fast ice. *Cold Reg. Sci. Technol.* **10**, 59–68.

Squire, V. A. 1984*c* Sea ice. *Sci. Prog.* **69**, 19–43.

Squire, V. A. 1984*d* How waves break up inshore fast ice. *Polar Rec.* **22**, 281–285.

Squire, V. A. 1989. Super-critical reflexion of ocean waves: a new factor in ice edge dynamics? *Ann. Glaciol.* **12**, 157–161.

Squire, V. A. & Fox, C. 1990 The wave structure in the seas off an ice edge. In *Ice technology II* (ed. P. Wadhams & T. K. S. Murthy), pp. 21–32. Cambridge: Springer-Verlag.

Squire, V. A. & Fox, C. 1991 The role of incoming waves in ice edge dynamics. *Annls Glaciol.* **15**, 96–100.

Squire, V. A. & Fox, C. 1992 On ice-coupled waves: a comparison of data and theory. In *Advances in Ice Technology: Proc. of the Third Int. Conf. on Ice Technology, 11–13 August 1992, Cambridge, MA, USA* (ed. T. K. S. Murthy, W. M. Sackinger & P. Wadhams), pp. 269–280. Computational Mechanics Publications.

Squire, V. A. & Martin, S. 1980. A field study of the physical properties, response to swell, and subsequent fracture of a single ice floe in the winter Bering Sea. *Univ. of Washington Depts of Atmos. Sci. and Oceanog. Rep.* **18**, 1–56.

Stoker, J. J. 1957 *Water waves. The mathematical theory with applications.* New York: Interscience.

Timokov, L. A. & Kheisin, D. E. 1987 *Dynamics of sea ice,* pp. 218–230. Leningrad: Gidrometeoizdat. (In Russian.)

Timoshenko, S. & Woinowsky-Krieger, S. 1970 *Theory of plates and shells,* 2nd edn. Singapore: McGraw-Hill.

Wadhams, P. 1973 The effect of a sea ice cover on ocean surface waves. Ph.D. thesis, University of Cambridge.

Wadhams, P. 1986 The seasonal ice zone. In *The geophysics of sea ice* (ed. N. Untersteiner), pp. 825–991. New York: Plenum Press.

Wadhams, P. & Holt, B. 1991 Waves in frazil and pancake ice and their detection in Seasat synthetic aperture radar imagery. *J. geophys. Res.* **96**, 8835–8852.

Weber, J. E. 1987 Wave attenuation and wave drift in the marginal ice zone. *J. phys. Oceanogr.* **17**, 2351–2361.

Weitz, M. & Keller, J. B. 1950 Reflection of water waves from floating ice in water of finite depth. *Communs pure appl. Math.* **3**, 305–318.

Received 10 August 1992; accepted 7 May 1993

PHILOSOPHICAL TRANSACTIONS OF THE ROYAL SOCIETY A MATHEMATICAL, PHYSICAL & ENGINEERING SCIENCES

PHILOSOPHICAL TRANSACTIONS OF THE ROYAL SOCIETY A MATHEMATICAL, PHYSICAL & ENGINEERING SCIENCES